
3-28-2019

Protein-Polymer Conjugates Synthesized Using Water-Soluble Azlactone-Functionalized Polymers Enable Receptor-Specific Cellular Uptake Toward Targeted Drug Delivery

Julia S. Kim
Smith College

Allison R. Sirois
Smith College


Analia J. Vazquez Cegla
Smith College

Eugenie Jumai'an
Smith College

Naomi Murata
Smith College

See next page for additional authors

Follow this and additional works at: https://scholarworks.smith.edu/chm_facpubs

 Part of the [Chemistry Commons](#), and the [Engineering Commons](#)

Recommended Citation

Kim, Julia S.; Sirois, Allison R.; Vazquez Cegla, Analia J.; Jumai'an, Eugenie; Murata, Naomi; Buck, Maren E.; and Moore, Sarah J., "Protein-Polymer Conjugates Synthesized Using Water-Soluble Azlactone-Functionalized Polymers Enable Receptor-Specific Cellular Uptake Toward Targeted Drug Delivery" (2019). Chemistry: Faculty Publications, Smith College, Northampton, MA. https://scholarworks.smith.edu/chm_facpubs/18

This Article has been accepted for inclusion in Chemistry: Faculty Publications by an authorized administrator of Smith ScholarWorks. For more information, please contact scholarworks@smith.edu

Authors

Julia S. Kim, Allison R. Sirois, Analia J. Vazquez Cegla, Eugenie Jumai'an, Naomi Murata, Maren E. Buck, and Sarah J. Moore

1 **TITLE**

2

3 **Protein-Polymer Conjugates Synthesized using Water-Soluble Azlactone-Functionalized**
4 **Polymers Enable Receptor-Specific Cellular Uptake towards Targeted Drug Delivery**

5

6 **AUTHORS**

7 Julia S. Kim[‡], Allison R. Sirois^{‡‡}, Analia J. Vazquez Cegla^{‡‡}, Eugenie Jumai'an[‡], Naomi Murata[⊥],
8 Maren E. Buck*[⊥], and Sarah J. Moore*^{‡‡}[∇]

9

10 [‡]Biochemistry Program, ^{‡‡}Picker Engineering Program, [⊥]Neuroscience Program, [⊥]Department of
11 Chemistry, and [∇]Department of Biological Sciences, Smith College, Northampton, Massachusetts
12 01063, United States

13 [‡]Molecular and Cellular Biology Program, University of Massachusetts Amherst, Amherst,
14 Massachusetts 01003, United States

15

16 *Corresponding authors:

17 Maren E. Buck: mbuck@smith.edu

18 Sarah J. Moore: sjmoore@smith.edu

19

20 **ABSTRACT**

21

22 Conjugation of proteins to drug-loaded polymeric structures is an attractive strategy for facilitating
23 target-specific drug delivery for a variety of clinical needs. Polymers currently available for
24 conjugation to proteins generally have limited chemical versatility for subsequent drug loading.
25 Many polymers that do have chemical functionality useful for drug loading are often insoluble in
26 water, making it difficult to synthesize functional protein-polymer conjugates for targeted drug
27 delivery. In this work, we demonstrate that reactive, azlactone-functionalized polymers can be
28 grafted to proteins, conjugated to a small molecule fluorophore, and subsequently internalized into
29 cells in a receptor-specific manner. Poly(2-vinyl-4,4-dimethylazlactone) (PVDMA) synthesized
30 using reversible addition-fragmentation transfer (RAFT) was modified post-polymerization with

31 substoichiometric equivalents of triethylene glycol monomethyl ether (mTEG) to yield reactive
32 water-soluble, azlactone-functionalized copolymers. These reactive polymers were then
33 conjugated to proteins holo-transferrin and ovotransferrin. Protein gel analysis verified successful
34 conjugation of proteins to polymer, and protein-polymer conjugates were subsequently purified
35 from unreacted proteins and polymers using size exclusion chromatography. Internalization
36 experiments using a breast cancer cell line that overexpresses the transferrin receptor on its surface
37 showed that the holo-transferrin-polymer conjugate was successfully internalized by cells in a
38 mechanism consistent with receptor-mediated endocytosis. Our approach to protein-polymer
39 conjugate synthesis offers a simple, tailorable strategy for preparing bioconjugates of interest for
40 a broad range of biomedical applications.

41

42 **INTRODUCTION**

43

44 Treatment of numerous diseases could benefit from improved options for targeted delivery of
45 drugs to disease-specific locations. Two important challenges in medicine for which targeted
46 delivery could significantly improve patient outcomes are delivery of therapeutics to the central
47 nervous system and delivery of chemotherapeutics selectively to tumor cells. The blood-brain
48 barrier (BBB) frequently prevents therapeutics from sufficiently accessing brain tissue, creating a
49 major bottleneck for developing treatments for diseases like Alzheimer's disease and brain
50 tumors.^{1,2} Often, drug development efforts for neurological diseases must focus on small molecule
51 candidates constrained by a set of physicochemical properties that can facilitate their passage
52 across the BBB.³ Receptor-mediated transcytosis (RMT) is a promising approach being developed
53 to use native transport pathways to shuttle larger therapeutic complexes across the BBB.^{4,5} Initial
54 reports of the ongoing clinical trials for the first RMT-based therapeutic to be used in humans have
55 been positive,⁶ encouraging continued development of therapeutics using RMT pathways for drug
56 delivery.

57 Specific targeting of chemotherapeutic agents to tumor cells could significantly reduce
58 toxic side effects that are currently caused by the systemic distribution of administered cytotoxic
59 drugs in the body.⁷ In recent years, substantial progress has been made toward the general goal of
60 targeted therapy using both passive and active targeting approaches.⁷ For example, antibody-drug
61 conjugates have been developed that rely on the specific targeting of tumor biomarkers using

62 antibodies to deliver a toxic payload to tumor cells.⁸⁻¹⁰ There are, however, challenges with finding
63 appropriate chemistries for conjugating the drug to the antibody, with continued need for improved
64 linkers between antibodies and their drug payload that do not inhibit antibody targeting and that
65 can release drug when the conjugate has reached the desired location.⁸ Inorganic and polymeric
66 nanocarriers have also been explored for both passive and active targeting.^{11,12} Although several
67 nanocarriers that passively target tumor cells have been approved for clinical use, no actively
68 targeted nanocarriers have advanced past clinical trials to date.¹² There remains a need for better
69 drug carriers that actively target pathological cells.

70 Active targeting of drug carriers to particular cell types is generally achieved by
71 conjugating a drug carrier to a ligand that binds specific cell-surface receptors. Drug carriers
72 include polymers and nanoparticles, and ligands can be proteins, peptides, or certain small
73 molecules.^{7,11,12} Proteins are particularly useful as targeting ligands because they exhibit precise
74 binding interactions with molecular partners. Protein engineering permits the manipulation of
75 these binding interactions such that a given targeting protein can be engineered to meet identified
76 design parameters, such as a desired affinity or binding epitope on the receptor.^{13,14} Consequently,
77 proteins, including antibodies and other protein classes, have found wide success on their own as
78 therapeutics for a variety of diseases.^{15,16} To be useful as a targeting ligand for drug delivery
79 applications, proteins that interact with a chosen disease marker need to be chemically coupled to
80 the drug to be delivered. Versatile and straightforward chemistries to conjugate drugs to proteins
81 are still needed.⁸ Polymers that link targeting proteins to drug molecules are a promising avenue
82 for developing a modular strategy for synthesizing targeted drug delivery molecules, where any
83 targeting protein of interest could be readily coupled to a drug molecule linked by a polymer that
84 couples to protein and to drug. Here, we report the development of protein-polymer conjugates
85 for targeted drug delivery applications.

86 Protein-polymer conjugates are being used in a variety of applications in medicine and
87 industry.¹⁷⁻¹⁹ The first generation of protein-polymer conjugates were comprised of polyethylene
88 glycol (PEG) attached to therapeutic proteins to extend the circulation time and reduce the
89 immunogenicity of the therapeutics. Over the past several decades, more than a dozen PEGylated
90 molecules have been approved for use in humans.²⁰⁻²² While PEG continues to be the leading
91 polymer for preparing clinically-relevant protein-polymer conjugates, PEG does have limitations,

92 such as non-degradability and potential immunogenicity,²³ that necessitate the development of
93 protein-polymer conjugates with an expanded selection of finely tuned functionalities.

94 Numerous advances in the development of protein-polymer conjugates with expanded
95 chemistries useful for biomedical applications have been reported in recent years.^{17–19,24,25} Strategies
96 for controlled polymerization^{19,24–26} and site-specific conjugation^{24,25,27–34} of polymers to proteins have
97 facilitated the synthesis of more well-defined protein-polymer conjugates. Site-specificity and
98 control of polymer synthesis are jointly achieved with approaches that grow polymers from
99 proteins functionalized with an initiator at a unique location in the protein sequence.^{24,31,33} While
100 growing polymers from appropriately-functionalized proteins, termed ‘grafting-from,’ affords
101 more easily purified conjugates,^{19,25,26} the grafting-from approach does limit to some extent the
102 chemistries that can be incorporated into the polymer structure. In addition, grafting-from requires
103 a new polymer to be synthesized each time the bioconjugate is prepared, which may lead to small
104 variations in the polymer structure, even when controlled methods are used. In a ‘grafting-to’
105 approach, preformed polymers bearing end-group or side-chain reactive functionality are
106 conjugated to proteins.^{25,35,36} A number of different chemistries have been used to facilitate grafting
107 of polymers to proteins, including polymers bearing amine-reactive functionality such as NHS-
108 esters or anhydrides,^{25,36,37} maleimide or dibromomaleimide functionality for reaction with cysteine
109 residues,^{25,36,38–40} and biorthogonal “click” reactions.^{25,34,36,41} Grafting-to permits incorporation of both
110 water-soluble and water-insoluble functionalities into the polymer structure. For example,
111 hydrophobic drugs are an important class of water-insoluble molecules that can be incorporated
112 into polymer structures when using the grafting-to approach. Grafting-to also allows conjugation
113 of a defined polymer structure to a variety of different proteins.

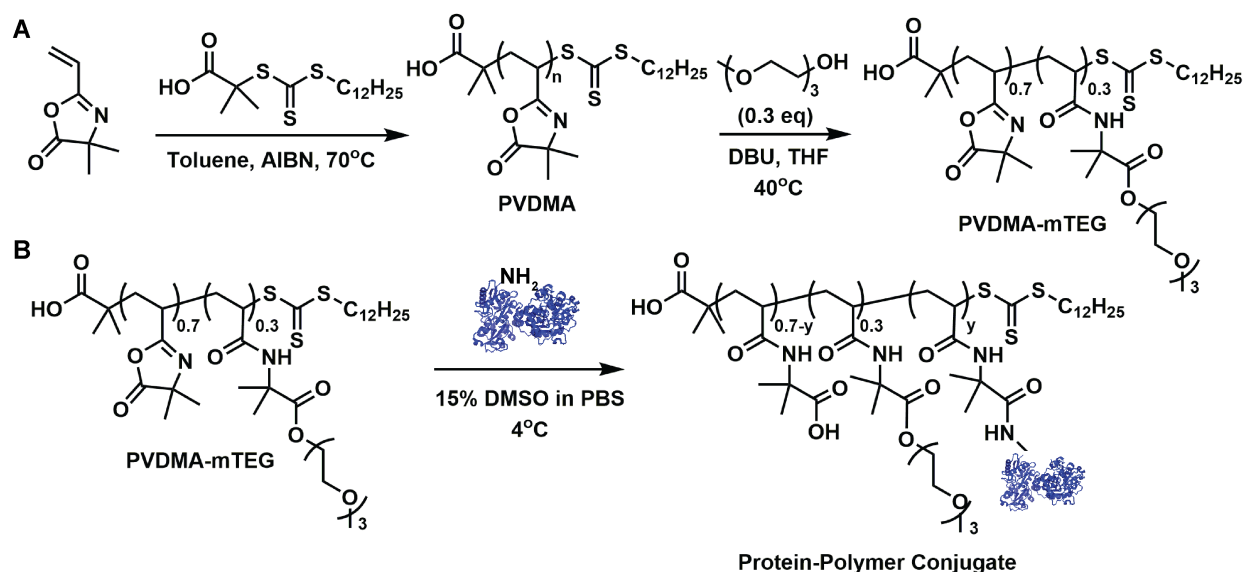
114 In the work reported here, we explored the use of side-chain reactive polymers for the
115 preparation of protein-polymer conjugates via a grafting-to approach. Side-chain reactive
116 polymers and their subsequent post-polymerization modification^{42–45} offer opportunities for
117 combinatorial synthesis of a broad range of polymer structures such that the influence of polymer
118 structure on bioconjugate properties can be easily explored.⁴⁶ Furthermore, these reactive groups
119 could be used to tether drug molecules to the scaffold before protein conjugation. In particular,
120 hydrophobic drugs can be more readily coupled to a polymer in organic solvent compared to
121 directly coupling a hydrophobic drug to a protein in aqueous solution. From a drug delivery
122 perspective, a polymer with a tunable number of sites for drug attachment is desirable because it

123 permits intentional selection of the number of drug molecules per protein-polymer conjugate. Such
124 flexibility in drug loading enables targeting an appropriate concentration in the body within a
125 particular drug's therapeutic window. It is then possible to achieve a sufficiently high
126 concentration of the drug at the disease site to have a desired therapeutic effect while remaining
127 below concentrations in the body that cause unacceptable toxicities. The ability to conjugate a
128 variety of active drug molecules directly to protein residues is more difficult than approaches that
129 use a delivery scaffold.

130 We used the reactive polymer poly(2-vinyl-4,4-dimethylazlactone) (PVDMA, Figure 1)
131 to prepare a series of protein-polymer conjugates. PVDMA is attractive for the preparation of
132 bioconjugates for several reasons. It can be synthesized from the vinyl monomer using a variety
133 of polymerization methods.^{43,45,47} In this current work, we synthesized PVDMA using reversible
134 addition-fragmentation chain transfer (RAFT) polymerization, which has been demonstrated
135 previously to yield well-defined azlactone-functionalized polymers (Figure 1A).⁴⁷⁻⁵⁰ Importantly
136 for this work, the five-membered lactone of PVDMA rapidly undergoes ring-opening reactions
137 with nucleophiles, such as amines and alcohols, including those found in native proteins.^{45,51} Thus,
138 a broad range of polymeric structures and bioconjugates can be readily synthesized starting from
139 the same template polymer. While azlactone-functionalized polymers have been used to
140 immobilize proteins on a variety of solid supports or thin films,^{45,51} only a few examples of soluble
141 protein-polymer conjugates have been reported.^{48,52,53} For example, Fontaine and coworkers
142 demonstrated the feasibility of using the azlactone functional group for conjugation of polymers
143 to lysozyme^{48,52} while Weeks et al. reported the conjugation of recombinant elastin-like polypeptides
144 to PVDMA.⁵³ However, because PVDMA is not inherently water-soluble, these previous reports
145 used organic solvents to conjugate the protein to the polymer.^{48,52,53}

146 In this work, we demonstrate the feasibility of synthesizing water-soluble, azlactone-
147 functionalized polymers and conjugating these reactive polymers to disease-relevant proteins.
148 Stover and coworkers reported the synthesis of water-soluble azlactone-functionalized polymers
149 through copolymerization of the azlactone monomer VDMA with a series of water-soluble
150 comonomers.⁵⁴ Others have demonstrated that PVDMA can be rendered water soluble by
151 exhaustive functionalization with appropriate side chain functionality.⁵⁵ In this report, we
152 functionalized PVDMA with substoichiometric amounts of triethylene glycol monomethyl ether
153 (abbreviated mTEG) to prepare reactive, water-soluble polymers (PVDMA-mTEG, Figure 1A).

154 This polymer readily conjugates to the proteins holo-transferrin (hTF) and ovotransferrin (OTF)
 155 in aqueous solution (Figure 1B). hTF represents a useful model protein for the development of
 156 targeted drug delivery scaffolds because the protein binds to and is internalized by cell-surface
 157 transferrin receptors (TFR) present on endothelial cells that comprise the blood brain barrier and
 158 expressed at high levels on many tumor cells.⁵⁶ hTF has also been used recently in the synthesis of
 159 protein-polymer conjugates and shown to facilitate receptor-specific targeting of conjugates to
 160 cells expressing the transferrin receptor.⁵⁷ Using confocal microscopy assays, we show that hTF-
 161 PVDMA-mTEG conjugates are internalized specifically into a tumor cell line that expresses TFR.
 162 This work exemplifies a modular approach for synthesizing protein-polymer conjugates and offers
 163 a new system that can be easily tailored for targeted drug delivery to a variety of disease-specific
 164 cell types.



166
 167
 168 **Figure 1. Synthesis of protein-polymer conjugates via a modular grafting-to approach using water-soluble,**
 169 **azlactone-functionalized polymers.** (A) PVDMA was synthesized by RAFT polymerization and functionalized with
 170 a substoichiometric equivalent of mTEG (0.3 molar eq. relative to repeat unit) to make the polymer soluble in water
 171 (PVDMA-mTEG). (B) PVDMA-mTEG can be subsequently grafted to a protein, including holo-transferrin shown
 172 here (PDB 3V83).

173
 174 **RESULTS AND DISCUSSION**

176 **Synthesis and Characterization of mTEG-functionalized PVDMA.** PVDMA was synthesized
 177 using RAFT polymerization⁸ (Figure 1A, step 1) to yield a well-defined homopolymer with $M_n =$
 178 13.1 kg/mol (Table 1). Water-soluble azlactone-functionalized polymers for protein conjugation
 179 were synthesized by treating the homopolymer with 0.3 equivalents of mTEG relative to the
 180 azlactone repeat unit (Figure 1A, step 2). DBU was used as a base catalyst and all reactions were
 181 stirred at 40 °C overnight. Figure 2A shows FT-IR spectra of PVDMA homopolymer and PVDMA
 182 treated with mTEG. The IR spectrum of PVDMA prior to functionalization (Figure 2A, black
 183 dashed curve) reveals peaks characteristic of the carbonyl (1820 cm^{-1}) and imine (1670 cm^{-1}) bonds
 184 of the azlactone ring. Treatment of PVDMA with 0.3 equivalents of mTEG (red curve) leads to a
 185 decrease in the carbonyl and imine peaks and the appearance of peaks at 1735 cm^{-1} (ester), 1650
 186 cm^{-1} (amide I), and 1540 cm^{-1} (amide II) that result from ring-opening of the lactone with an alcohol
 187 nucleophile. Quantitative analysis of mTEG functionalization using NMR spectroscopy revealed
 188 that mTEG was incorporated into the polymer in nearly quantitative yield (Table 1). GPC analysis
 189 of PVDMA functionalized with mTEG revealed an increase in molecular weight consistent with
 190 functionalization of the polymer (Table 1). GPC analysis also confirmed that no polymer
 191 crosslinking occurred during treatment with mTEG, based on observing no increase in dispersity
 192 comparing polymer before and after mTEG functionalization. The absence of crosslinking is
 193 expected since mTEG only has one nucleophile that is reactive with the azlactone group. Finally,
 194 while PVDMA can be functionalized with larger amounts of mTEG, polymers modified with 0.3
 195 equivalents proved to be soluble in water. Thus, this polymer, referred to hereafter simply as
 196 PVDMA-mTEG, was used for all experiments described here to provide the greatest number of
 197 remaining reactive groups in the polymer for additional modifications and protein conjugation.

198

199 **Table 1. Characterization of polymers by NMR spectroscopy and GPC.**

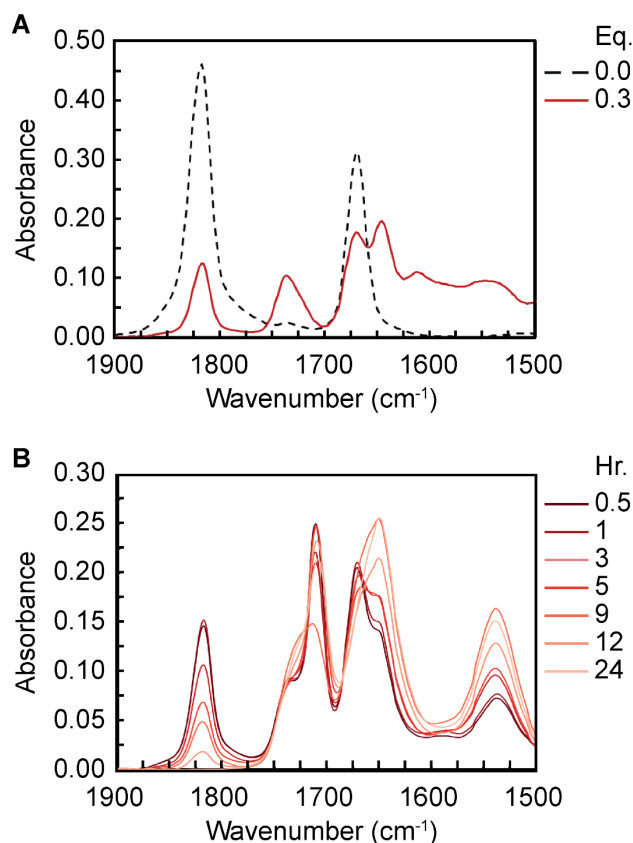
Polymer Name	mTEG eq. ^a	Actual mTEG ^b	M_n (kg/mol) ^c	\mathcal{D}^c
PVDMA	0	0	13.1	1.35
PVDMA-mTEG	0.3	0.28	20.0	1.25

200

201 ^aMolar equivalents of mTEG relative to the azlactone repeat unit in the reaction. ^bMolar equivalents of mTEG
 202 incorporated into the polymer was determined using ¹H NMR spectroscopy. 4-Iodoanisole was added as an internal
 203 standard and mTEG functionalization was determined by comparing the integration of the ester peak at 4.22 ppm to
 204 the integration of the peak at 6.67 ppm arising from 4-iodoanisole. ^cNumber average molecular weight and dispersity
 205 determined by GPC in THF measured against polystyrene standards.

206
207
208
209
210
211
212
213
214
215
216
217
218
219
220
221

One potential challenge associated with using the azlactone moiety for protein conjugation in aqueous solution is that these groups are susceptible to hydrolysis. However, hydrolysis reactions are typically slower than reactions of azlactones with amines. Furthermore, azlactone groups have been shown to persist for several hours in water when copolymerized with certain water soluble monomers.⁵⁴ To qualitatively characterize the rate of hydrolysis of PVDMA-mTEG, we acquired IR spectra of a polymer dissolved in water (Figure 2B) over time. The series of spectra shown in Figure 2B reveal that the lactone carbonyl peak (1820 cm^{-1}) persists for at least 12 hours. The polymer fully hydrolyzes in 24 hours as evidenced by the complete disappearance of the lactone carbonyl peak at 1820 cm^{-1} (Figure 2B). Based on these data, we hypothesized that, following functionalization with mTEG, sufficient azlactones would remain on the polymer to permit reaction with amines on a protein (i.e., the N-terminus or lysine residues), but that all residual azlactone groups would fully hydrolyze during or after protein conjugation. This latter hydrolysis reaction is desirable in order to avoid unwanted reactions of the polymer with proteins on cells in subsequent cell internalization experiments.



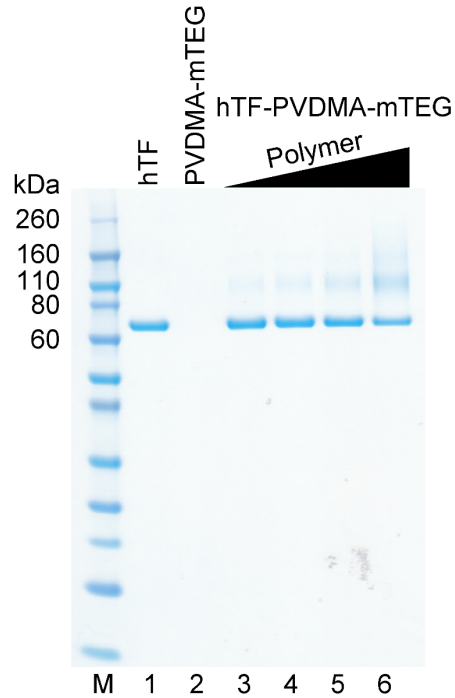
222
 223 **Figure 2. Water-soluble, azlactone-functionalized copolymers can be synthesized by post-polymerization**
 224 **modification of PVDMA.** (A) FT-IR spectra of PVDMA (black dashed curve) and PVDMA modified with 0.3 molar
 225 equivalents (Eq.) of mTEG relative to the repeat unit (red curve). The peaks at 1820 cm⁻¹ (carbonyl) and 1670 cm⁻¹
 226 (imine) are characteristic of the azlactone ring. Ring opening of the lactone with an alcohol nucleophile results in the
 227 disappearance of the azlactone peaks and the appearance of ester (1720 cm⁻¹), amide I (1650 cm⁻¹), and amide II (1540
 228 cm⁻¹) peaks. (B) FT-IR spectra as a function of time of PVDMA-mTEG incubated in water. FT-IR spectra revealed
 229 the disappearance of the azlactone carbonyl (1820 cm⁻¹) peak and an increase in the peaks at 1735 cm⁻¹ (ester+carboxylic
 230 acid carbonyl), 1650 cm⁻¹ (amide I), and 1540 cm⁻¹ (amide II). The strong peak at 1710 cm⁻¹ corresponds to acetone,
 231 which was used to cast the polymer film on the ATR crystal. The legend refers to time in hours following dissolution
 232 of PVDMA-mTEG in water.

233
 234 ***Protein Holo-transferrin Conjugates to PVDMA-mTEG.*** For our initial experiments, holo-
 235 transferrin (hTF) was selected to determine the feasibility of conjugating proteins to PVDMA-
 236 mTEG. hTF is an 80 kDa glycoprotein containing 58 lysine residues (UniProt P02787) and is the
 237 native protein ligand for the transferrin receptor (TFR).⁵⁶ Upon binding its receptor, hTF gets
 238 internalized into cells through receptor-mediated endocytosis. The hTF-TFR interaction is of
 239 interest for a variety of clinical applications.⁵⁶ For example, receptor-mediated transcytosis

240 facilitated by TFR has been studied for drug delivery across the blood-brain barrier to the central
241 nervous system.⁵⁹ TFR is also overexpressed in many cancers, which makes it an interesting
242 receptor system to be used as a model for targeted drug delivery to tumor cells.⁶⁰ Because PVDMA
243 reacts readily with the primary amines in the N-termini and lysine residues in proteins,^{45,51} hTF
244 provides ample reactive sites for conjugation.

245 Conjugates were prepared by incubating PVDMA-mTEG with hTF in phosphate buffered
246 saline (PBS) containing 15% v/v DMSO at 4 °C. Low concentrations of DMSO are commonly
247 used to facilitate conjugation of reactive small molecules and polymers to proteins.^{37,61} We examined
248 a range of molar ratios of polymer:protein for hTF conjugation reactions. Successful conjugation
249 of polymer to protein was assessed using SDS-PAGE (Figure 3). Lane 1 contains pure hTF protein
250 with no polymer. Lane 2 contains PVDMA-mTEG polymer with no protein, which is not detected
251 by the protein gel stain. Lanes 3 through 6 include conjugation reactions in which the amount of
252 protein was kept constant while the amount of PVDMA-mTEG was increased. Lane 3 reveals
253 the presence of a faint band at higher molecular weight than the hTF protein band. The apparent
254 molecular weight of this band is consistent with the molecular weight of one protein and one
255 polymer molecule, suggesting the formation of conjugates at a 1:1 molar ratio of protein:polymer.
256 With higher amounts of polymer in the conjugation reaction (Figure 3, lane 4-6), we observe a
257 band at a molecular weight consistent with a protein:polymer molar ratio of 1:2. Increasing the
258 molar amount of polymer relative to protein resulted in a darkening of this higher molecular weight
259 band. We do not observe any protein bands at a molecular weight that suggests two or more
260 proteins in a conjugate molecule with at least one polymer. While all reactions show residual
261 unreacted protein, as demonstrated by the presence of the original protein band in lanes 3-6, the
262 intensities of these bands are increasingly reduced compared to the intensity of the protein only
263 sample shown in lane 1. The same amount of total protein was loaded into lanes 1 and 3-6, and,
264 therefore, reduction in the original protein band intensity further suggests successful protein-
265 polymer conjugation. Taken together, these data demonstrate that hTF conjugates to PVDMA-
266 mTEG through reactive, azlactone functionality in aqueous solution.

267



268
269

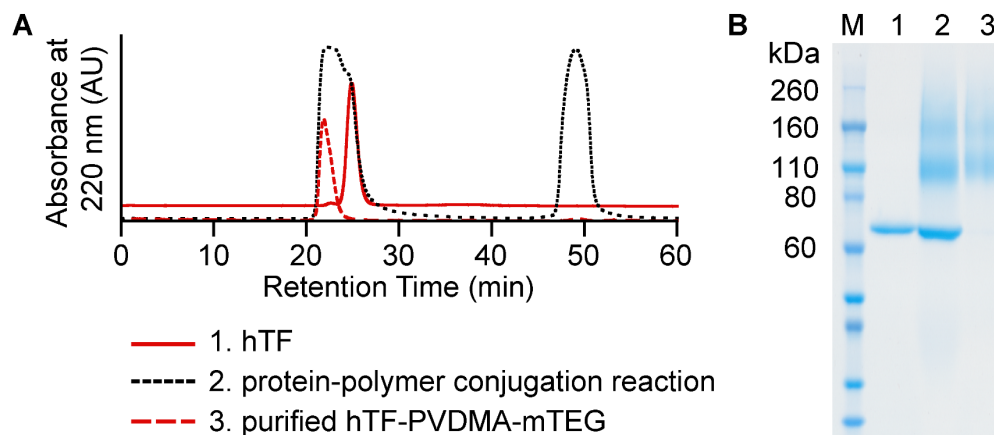
270 **Figure 3. Protein hTF conjugates to PVDMA-mTEG.** Holo-transferrin (hTF) conjugates to PVDMA-mTEG in
 271 aqueous solution. The appearance of higher molecular weight bands and decrease in intensity of primary protein band
 272 indicate protein conjugation to polymer. Protein amounts in each lane were held constant. Lane 1 contains protein
 273 only, lane 2 contains PVDMA-mTEG only. Lanes 3-6 contain unpurified protein-polymer conjugation reactions at
 274 an increasing amount of polymer relative to protein, keeping amount of protein constant. Molar ratios of protein to
 275 polymer molecules in reactions are: lane 3 = 1:5; lane 4 = 1:10; lane 5 = 1:20; lane 6 = 1:50. Samples are not reduced.
 276 Apparent molecular weights of the two protein-polymer conjugate bands are most consistent with protein:polymer
 277 conjugate ratios of 1:1 and 1:2.

278

279 ***Protein-Polymer Conjugates can be Purified by Size Exclusion Chromatography.*** Prior to use
 280 in receptor targeting experiments with a human cell line, protein-polymer conjugates were purified
 281 from unreacted protein and unreacted polymer. Samples were first concentrated and purified from
 282 low molecular weight species by using a centrifugal filtration device with a 10 kDa molecular
 283 weight cut-off (MWCO) before being loaded onto a size exclusion chromatography (SEC) column.
 284 Samples were analyzed by detecting absorbance at 220 nm. Pure hTF protein exhibits a single
 285 narrow peak on SEC (Figure 4A, red solid curve). PVDMA-mTEG exhibits a broad high
 286 molecular weight peak and a narrow low molecular weight peak (Figure S1A). Unpurified protein-
 287 polymer conjugates eluted at shorter retention times (i.e., higher molecular weight) relative to hTF

288 only and included low molecular weight species similar to polymer only samples (Figure 4A, black
289 dashed curve). We were able to collect the high molecular weight protein-polymer conjugate peak,
290 which no longer contained unreacted protein when analyzed by SEC (Figure 4A, red dashed curve)
291 and SDS-PAGE (Figure 4B). Because the molecular weight of the polymer is less than the
292 molecular weight of the protein, we anticipate that most or all of the unreacted polymer was
293 removed through SEC purification. However, because polymer alone does not stain on the protein
294 gel, it is possible that some unreacted polymer remains following SEC purification.

295 The purified protein-polymer conjugates contained a mixture of conjugates at
296 protein:polymer ratios of 1:1 and 1:2 (Figure 4B). On SEC, we did not observe any products of
297 the conjugation reaction that would suggest more than one protein per conjugate, based on analysis
298 of retention time of the protein-polymer conjugation reactions. However, it is possible that any
299 conjugates with two proteins joined by one or more polymers may elute at a longer retention time
300 than would be predicted for a globular protein of the same molecular weight, so it remains possible
301 that some protein-polymer conjugates containing two proteins exist in our reaction mixture. The
302 lack of molecules in the conjugation reaction mixture eluting at less than 20 min retention time
303 does conclusively indicate a lack of higher order aggregates.

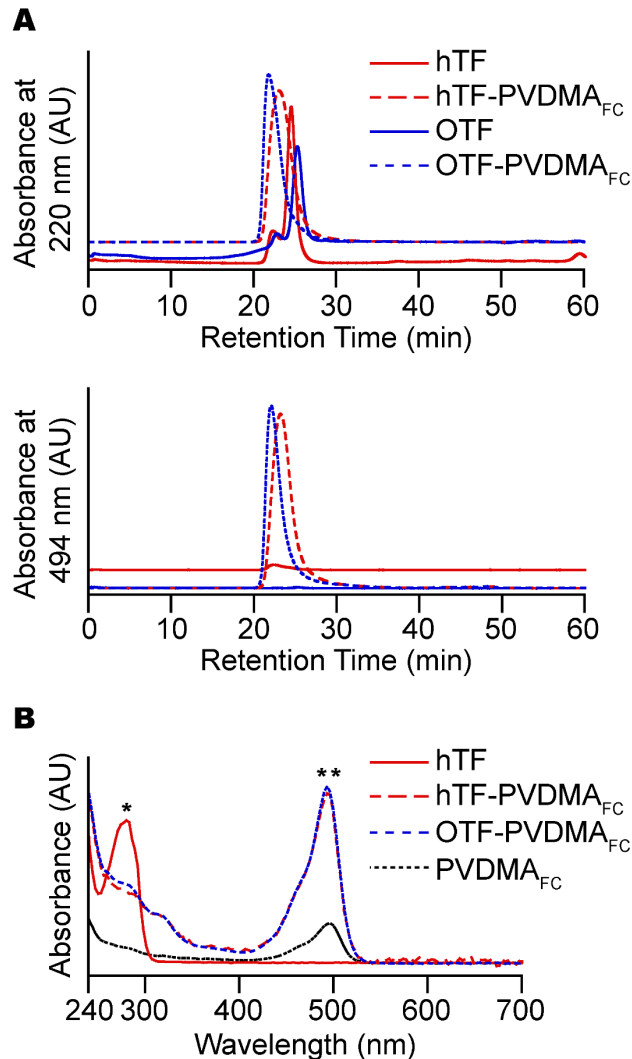


304
305 **Figure 4. Purification of hTF-PVDMA-mTEG conjugates.** (A) SEC was used to analyze and purify hTF-PVDMA-
306 mTEG conjugates from unreacted hTF and from unreacted PVDMA-mTEG. Larger molecules have a shorter retention
307 time. Pure hTF protein (red solid line) exhibits a single narrow peak for absorbance at 220 nm. The protein-polymer
308 conjugation reaction (black dashed line) has overlapping peaks that include an unreacted hTF peak and a new larger
309 molecule with shorter retention time consistent with protein-polymer conjugates, as well as a low molecular weight
310 peak from polymer byproducts. There are no peaks in the conjugation reaction that elute < 20 min, indicating the
311 absence of higher order protein-polymer aggregates. Following collection of the protein-polymer conjugate peak and
312 reinjection onto SEC, a narrow peak is observed as purified hTF-PVDMA-mTEG (red dashed line). (B) SDS-PAGE

313 analysis of hTF (lane 1), protein-polymer conjugation reaction before purification (lane 2), and SEC purified hTF-
314 PVDMA-mTEG conjugate (lane 3) demonstrates successful purification of conjugates using SEC. In the purified
315 product (lane 3), unreacted hTF is absent. Polymers are at lower molecular weight than hTF and should therefore also
316 be removed by SEC purification. Molecular weights of purified conjugates are consistent with protein:polymer ratios
317 of 1:1 and 1:2. Samples are not reduced.

318
319 ***Fluorescent, Hydrophobic Small Molecule can be Coupled to PVDMA-mTEG Prior to Polymer***

320 ***Conjugation to Protein.*** To permit visualization of protein-polymer conjugates in the presence of
321 cells using fluorescence imaging techniques, we fluorescently labeled PVDMA-mTEG with the
322 amine-functionalized fluorophore fluorescein cadaverine (FC, labeled polymer denoted as
323 PVDMA_{FC}-mTEG). Coupling a small molecule fluorophore directly to the polymer models a way
324 in which drugs could be tethered to the polymer for future drug delivery applications. FC was
325 reacted with PVDMA-mTEG in DMSO in a molar ratio of FC to VDMA monomer such that 1-2
326 molecules of FC were coupled to each polymer chain. Many small molecule drugs are
327 hydrophobic, and the ability to couple drugs to polymer in organic solvent prior to an aqueous
328 reaction conjugating polymer to protein is an advantage of our approach. We then coupled the
329 fluorescently labeled PVDMA_{FC}-mTEG to hTF and to the protein ovotransferrin (OTF). OTF is the
330 chicken homolog of human transferrin. It has the same overall structure and size as human hTF,
331 but is sufficiently distinct in sequence that it does not bind to human TFR⁶², making OTF conjugates
332 a suitable negative control for TFR binding and internalization experiments. FC labeled protein-
333 polymer conjugates were purified from unreacted molecules by SEC as described above, yielding
334 a single pure peak when analyzed by SEC (Figure 5A). The peak exhibits absorbance at 220 nm
335 (Figure 5A, top) and at 494 nm (Figure 5A, bottom). Absorbance at 494 nm is characteristic of the
336 fluorophore, and is absent in the sample of pure protein, indicating successful conjugation of FC
337 to polymer, and subsequent conjugation of PVDMA_{FC}-mTEG to protein. Analysis of the purified
338 FC labeled protein-polymer conjugates using UV-visible spectroscopy resulted in absorbance
339 peaks at 280 nm and 494 nm (Figure 5B). In pure hTF protein, there is only an absorbance peak
340 at 280 nm. In PVDMA-mTEG without FC conjugation, we see no absorbance peaks in the UV-
341 visible range, as expected (Figure S1B). The presence of the 494 nm absorbance peak in the FC-
342 coupled PVDMA-mTEG and in the purified protein-polymer conjugates confirms that FC was
343 successfully conjugated to PVDMA-mTEG and that PVDMA_{FC}-mTEG subsequently was able to
344 be conjugated to hTF and OTF.



346

347 **Figure 5. Fluorescent, hydrophobic small molecule can be coupled to polymer and protein-polymer**
 348 **conjugates.** Small molecule fluorophore fluoresceine cadaverine (FC) was conjugated to PVDMA-mTEG, and the
 349 resulting PVDMA_{FC}-mTEG was conjugated to hTF or OTF. (A) SEC was used to purify and analyze hTF-PVDMA_{FC}-
 350 mTEG and OTF-PVDMA_{FC}-mTEG conjugates from unreacted component molecules. A single peak for hTF-
 351 PVDMA_{FC} and for OTF-PVDMA_{FC} with retention time shorter than for the corresponding protein alone, and with
 352 absorbance at 220 nm (top) and for 494 nm (bottom), demonstrates small molecule fluorophore incorporation into
 353 the purified protein-polymer conjugates. Protein alone does not absorb at 494 nm. The FC molecule absorbs at 494
 354 nm. (B) UV-Vis absorption spectra for hTF protein, PVDMA_{FC}-mTEG, purified hTF-PVDMA_{FC}-mTEG, and purified
 355 OTF-PVDMA_{FC}-mTEG. The characteristic absorption peaks for protein (*) and FC (**) are indicated at 280 nm and
 356 494 nm, respectively. Concentrations of samples differ, resulting in different heights of absorbance peaks.

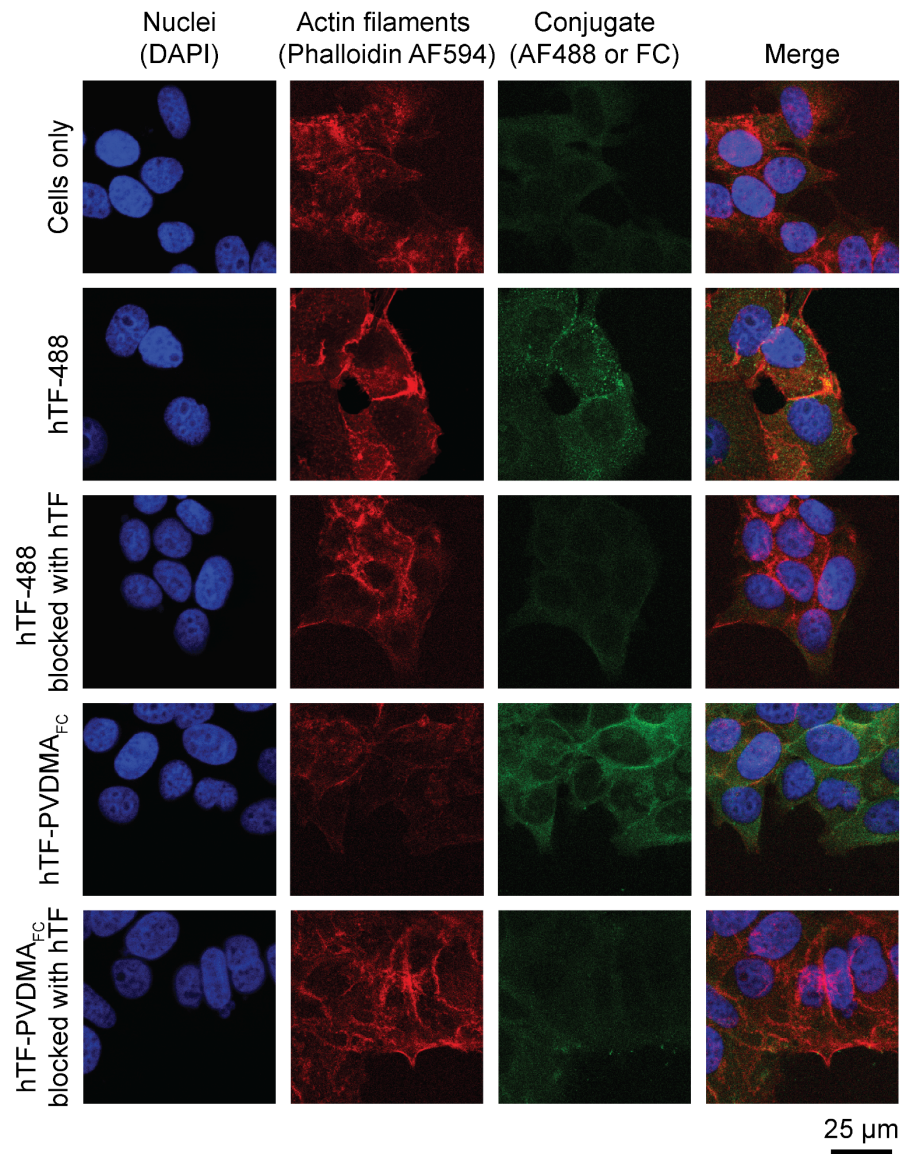
357

358 ***Internalization of Protein-polymer Conjugates into Cells is Receptor-specific.*** We next
359 determined that protein-polymer conjugates are specifically internalized through receptor-
360 mediated endocytosis. MCF-7 breast cancer cells have been shown to overexpress the transferrin
361 receptor on their surface and have been previously used to study internalization of molecules
362 targeted to TFR.^{63,64} Flow cytometry with an antibody that recognizes human TFR confirmed high
363 levels of surface TFR expression on the MCF-7 cell line (Figure S2A). A titration binding assay
364 was performed with fluorescently labeled hTF and MCF-7 cells to determine an appropriate
365 concentration of protein or protein-polymer conjugate for cell internalization experiments. We
366 determined a dissociation constant (K_d) of 10 ± 5 nM (Figure S2B), which is consistent with
367 previously reported values.⁶⁵ A biological interpretation of the K_d is that half of the receptors are
368 occupied by ligand when the ligand concentration is equal to the K_d . In subsequent conjugate
369 internalization experiments, we incubated MCF-7 cells with 10 nM of conjugates to provide ample
370 ligand to visualize receptor-specific internalization, without overwhelming the receptor
371 internalization machinery.

372 All internalization experiments were conducted by incubating protein-polymer conjugate
373 samples or control samples with MCF-7 cells for 1 h at 37 °C in culture media without serum.
374 These conditions are on the time scale and at the relevant temperature for receptor-mediated
375 endocytosis to occur in MCF-7 cells.⁶⁵ Prior to imaging, all cells were stained with phalloidin
376 (shown by red fluorescence), which binds to actin filaments and demarcates cell boundaries, and
377 DAPI (shown by blue fluorescence), which stains cell nuclei. All protein, protein-polymer, and
378 polymer samples were fluorescently labeled with either Alexa Fluor 488 (AF488, samples with
379 protein only) or FC (all polymer-containing samples) and are shown as green fluorescence.

380 Row 1 of Figure 6 shows confocal microscopy images for MCF-7 cells stained with DAPI
381 and phalloidin to identify nuclei and actin filaments, but with no protein, polymer, or conjugates
382 added; these images show the level of background cellular autofluorescence in the channel that
383 was used to visualize targeting molecules. Row 2 of Figure 6 shows confocal microscopy images
384 for MCF-7 cells incubated with 10 nM hTF-488. The green channel and merged images show
385 punctate regions of green fluorescence distributed throughout the cell body (cell boundaries shown
386 in red channel), indicating internalization of the protein. The presence of punctate structures is
387 consistent with protein localized to endosomes after receptor-mediated endocytosis. When treated
388 with increasing concentrations of hTF-488, MCF-7 cells show increased levels of internalization

389 (Figure S3), also consistent with receptor-mediated endocytosis. To further demonstrate that
390 ligand-receptor interactions are necessary for internalization, we conducted a competition
391 experiment in which cells were treated with hTF-488 (10 nM) and a 1000-fold excess of unlabeled
392 hTF (10 μ M) (Figure 6, row 3). As expected, when labeled protein was in competition with an
393 excess of unlabeled protein, green fluorescence signal within the cell body was reduced to the level
394 of background autofluorescence (Figure 6, row 3). The results of these control experiments
395 demonstrate that hTF is internalized into our MCF-7 cells via a mechanism consistent with
396 receptor-mediated endocytosis.
397



398

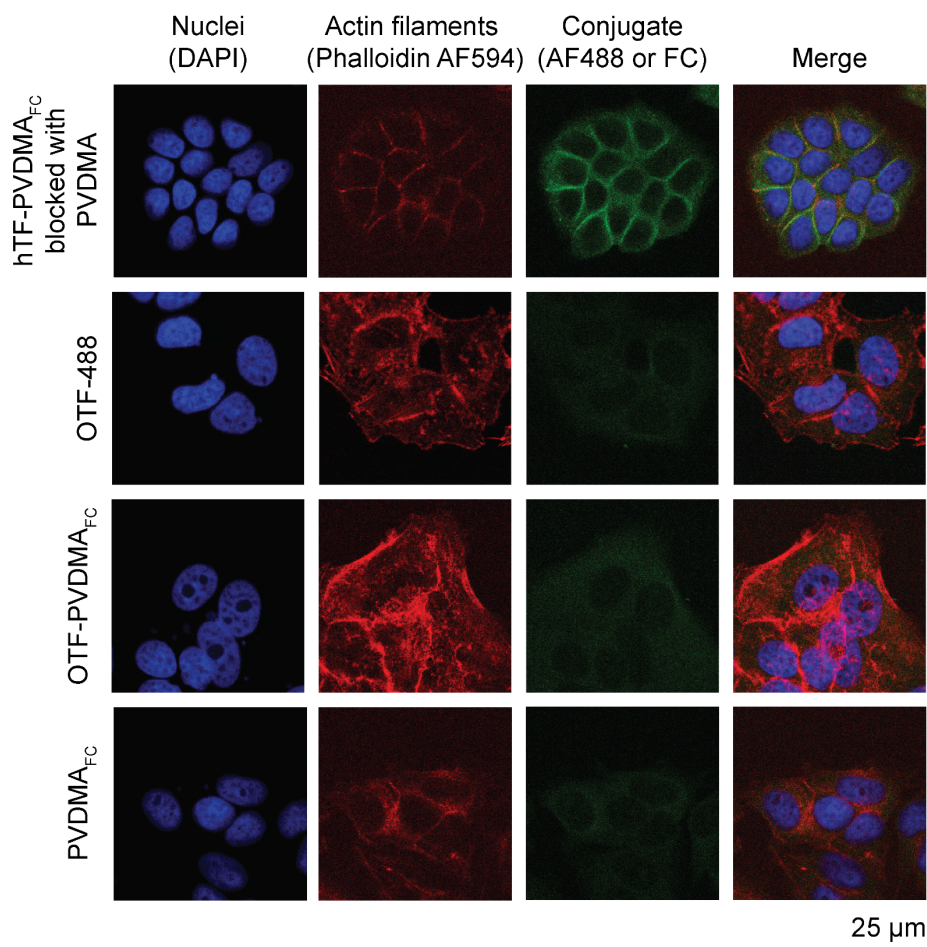
399 **Figure 6. hTF-PVDMA_{rc}-mTEG targeted protein-polymer conjugates are internalized into MCF-7 cells**
400 **through receptor-specific interactions.** Cells not treated with protein or protein-polymer conjugate exhibit a low
401 background level of autofluorescence in the green channel (row 1). As a positive control, holo-transferrin protein
402 directly labeled with fluorophore (hTF-488) is internalized into MCF-7 cells that express transferrin receptor, as seen
403 by green punctate structures throughout the cell body (row 2). hTF-488 internalization can be blocked by competition
404 with an excess of unlabeled hTF protein (row 3). Fluorescently labeled polymer conjugated to human holo-transferrin
405 (hTF-PVDMA_{rc}-mTEG) is similarly internalized into the cell line (row 4). Competition between hTF-PVDMA_{rc}-
406 mTEG and excess unlabeled hTF blocks internalization and reduces signal to the level of autofluorescence (row 5),
407 indicating that binding and internalization of the protein-polymer conjugate is mediated by specific interactions
408 between hTF its receptor, TFR. Cells were incubated with samples for 1 h at 37 °C to allow receptor-mediated
409 internalization to occur. Blue indicates DAPI stain for cell nuclei; red indicates phalloidin conjugated to Alexa Fluor
410 594, which stains actin filaments and helps to identify cell boundaries; and green indicates the protein or protein-
411 polymer conjugate, with positive control protein labeled with Alexa Fluor 488 or polymer labeled with fluorescein
412 cadaverine. Scale bar shown applies to all images.

413
414 Confocal microscopy images of MCF-7 cells treated with hTF conjugated to PVDMA_{rc}-
415 mTEG (Figure 6, row 4) exhibited punctate regions of green fluorescence throughout the cell body,
416 similar to results observed with hTF-488. These results demonstrate successful internalization of
417 the conjugates. A competition experiment similar to that described above for hTF-488 was
418 performed in which cells were treated with hTF-PVDMA_{rc}-mTEG conjugate in the presence of
419 1000-fold excess (10 μ M) unlabeled hTF. The green channel and merged confocal microscopy
420 images for this experiment (Figure 6, row 5) reveal the reduction of green signal to the level of
421 autofluorescence, indicating that the internalization of hTF-targeted protein-polymer conjugates is
422 dependent on specific binding of hTF to TFR. Internalization of hTF-488 and of hTF-PVDMA_{rc}-
423 mTEG molecules was further demonstrated by collecting a series of images from neighboring
424 confocal planes of clusters of cells, termed z-stacks, confirming that green fluorescence is present
425 within cells, rather than on the cell surface (Supporting Information Video 1 and Video 2).

426 We explored whether non-specific polymer interactions substantially contributed to the
427 binding and internalization signal we observed for hTF-PVDMA_{rc}-mTEG (Figure 7). We co-
428 incubated hTF-PVDMA_{rc}-mTEG with an excess of unlabeled PVDMA-mTEG, and observed no
429 noticeable reduction in signal, suggesting that non-specific interactions of the polymer with the
430 cell surface are not necessary for binding and internalization (Figure 7, row 1). To further confirm
431 that specific ligand-receptor interactions are required for internalization, we examined potential

432 binding and internalization of the negative control protein-polymer conjugate, OTF-PVDMA_{FC}-
 433 mTEG, which was not expected to bind any MCF-7 cell surface receptors. OTF is a chicken
 434 transferrin, and MCF-7 cells express human TFR. We did not observe any MCF-7 cell binding or
 435 internalization of OTF protein directly labeled with AF488 (Figure 7, row 2). Similarly, we also
 436 did not observe MCF-7 cell binding or internalization of the non-targeted OTF-PVDMA_{FC}-mTEG
 437 (Figure 7, row 3). Finally, fluorescently labeled polymer not conjugated to any protein (PVDMA_{FC}-
 438 mTEG) does not adhere to or internalize into MCF-7 cells (Figure 7, row 4). These results provide
 439 further confirmation that hTF-PVDMA_{FC}-mTEG conjugates are internalized via specific
 440 interactions of the hTF ligand with cell surface receptor TFR, rather than through non-specific
 441 interactions of polymer with the cells.

442



443

444 **Figure 7. Polymer does not cause non-specific cell staining for protein-polymer conjugates.** Including excess
 445 unlabeled polymer during the internalization period of hTF-PVDMA_{FC}-mTEG does not block receptor-specific

446 internalization of hTF-PVDMA_{re}-mTEG (row 1). MCF-7 cells neither bind nor internalize non-targeted chicken
447 ovotransferrin protein labeled directly with fluorophore (OTF-488) (row 2) or fluorescently labeled OTF-polymer
448 conjugates (OTF-PVDMA_{re}-mTEG) (row 3). Fluorescently labeled polymer not conjugated to protein (PVDMA_{re}-
449 mTEG) similarly does not stain cells (row 4). Blue indicates DAPI stain for cell nuclei; red indicates phalloidin
450 conjugated to Alexa Fluor 594, which stains actin filaments and helps to identify cell boundaries; and green indicates
451 the protein or protein-polymer conjugate, with OTF control protein labeled with Alexa Fluor 488 and polymer labeled
452 with fluorescein cadaverine. Scale bar shown applies to all images.

453
454 When conjugating polymers to proteins, there is the risk that the polymer will destabilize
455 the protein structure, or that the polymer will sterically block the interaction of a protein ligand
456 with its receptor, rendering the protein-polymer conjugate irrelevant for the intended application.
457 Importantly, the protein-polymer conjugate internalization experiments we have conducted
458 demonstrate that hTF protein maintains its ability to bind and be internalized by TFR when
459 conjugated to PVDMA-mTEG, suggesting that hTF maintains its structure and function when
460 conjugated to PVDMA-mTEG.

461
462 **CONCLUSION**

463
464 We have developed a new, modular strategy for conjugating diverse proteins to hydrophilic
465 polymers using the reactive, azlactone-functionalized polymer PVDMA with the goal of
466 developing conjugates for applications in targeted drug delivery. In our approach, we first
467 functionalized PVDMA with mTEG to render the polymer water-soluble. We demonstrated the
468 conjugation of this reactive polymer with proteins in aqueous solution. When the targeting protein
469 holo-transferrin was conjugated to a fluorescently-labeled analog of PVDMA-mTEG, protein-
470 polymer conjugates were internalized into tumor cells expressing the transferrin receptor in a
471 receptor-specific manner.

472 Internalization of hTF-PVDMA-mTEG conjugates into human cells expressing TFR has
473 implications for targeted delivery to the central nervous system and to tumor cells with
474 overexpressed receptors.^{4,56,60,66-68} Our approach to synthesizing protein-polymer complexes for drug
475 delivery could be extended to encompass protein ligands that bind other receptors relevant for a
476 variety of clinical needs to generate protein-polymer-drug conjugates for diverse targeted drug
477 delivery applications. Although in this initial report proteins were conjugated to PVDMA through

478 primary amines contained naturally in the native protein sequences, both the targeting protein and
479 the polymer could be further modified for site-specific conjugation reactions.

480 While the experiments described here focused on mTEG-modified PVDMA, this post-
481 polymerization modification approach to the synthesis of multifunctional bioconjugates permits
482 rapid and straightforward access to a broad range of macromolecular structures without requiring
483 the synthesis of new polymers each time a new structure is to be investigated. For example, diverse
484 side chain chemistries and degrees of functionalization can readily be explored. In addition,
485 because the polymer modification reactions are conducted initially in organic solvents, non-water
486 soluble functionality, such as hydrophobic drugs, may be incorporated into the polymer prior to
487 conjugation to the proteins. The synthetic versatility of PVDMA and the ease with which it can be
488 conjugated to proteins offers opportunities for preparing a range of bioconjugates tailored to
489 specific biomedical applications.

490

491 **EXPERIMENTAL PROCEDURES**

492

493 **Materials.** Triethylene glycol monomethyl ether (mTEG), 1,8-diazabicyclo[5.4.0]undec-7-ene
494 (DBU), 2,2'-azobis(2-methylpropionitrile) (AIBN), 2-(dodecylthiocarbonothioylthio)-2-
495 methylpropionic acid, ovotransferrin (OTF), 4-iodoanisole, and anhydrous dioxane were
496 purchased from Sigma Aldrich and used without further purification unless otherwise noted. The
497 monomer 2-vinyl-4,4-dimethylazlactone (VDMA) was synthesized as previously described.⁶⁹
498 Fluorescein cadaverine (FC) was purchased from Biotium. Alexa Fluor 488 tetrafluorophenyl
499 ester, NuPAGE 4-12% Bis-Tris gels, MES buffer, and LDS buffer were purchased from
500 ThermoFisher Scientific. Inhibitor removal resin was purchased from Alfa Aesar. Holo-transferrin
501 (HTf, Cat.: 616397) was purchased from CalBiochem. PBS (10X) were purchased from Fisher
502 Scientific. THF was purified using alumina drying columns. All other solvents were purchased
503 from Pharmco-AAPER (Brookfield, CT). Deuterated DMSO (DMSO-*d*₆) and deuterated
504 chloroform (CDCl₃) were purchased from Cambridge Isotope Laboratories, Inc. Dulbecco's
505 Modified Eagle's Medium (DMEM) was purchased from ATCC, and all other cell culture reagents
506 were obtained from Gibco. Phalloidin conjugated to Alexa Flour 594 was purchased from Thermo
507 Fisher, formaldehyde as a 3.7% solution in PBS was from Fisher Scientific, and Vectashield
508 mounting medium with DAPI was from Vector Labs.

509

510 **General Considerations.** ¹H-NMR spectra were collected on a Bruker 500 MHz NMR
511 spectrometer. Attenuated total reflectance infrared (ATR-IR) spectra were obtained using a Bruker
512 ALPHA FTIR spectrometer and analyzed using OPUS software version 7.5. Gel-permeation
513 chromatography (GPC) was performed on an Agilent 1260 GPC instrument equipped with PLgel
514 Mixed C and Mixed D columns and an RI detector, operating in THF at 40 °C with a flow rate of
515 1 mL/min. Molecular weights and dispersities were measured against polystyrene calibration
516 standards. SEC was performed using a Superdex 75 10/300 GL column (GE) and an Agilent 1200
517 series liquid chromatography system. Flow cytometry was performed on a Guava easyCyte flow
518 cytometer (Millipore-Sigma). Laser scanning confocal microscopy images were acquired on a
519 Leica TCS SP5 laser scanning confocal microscope and analyzed using LAS AF software version
520 2.7.3.9723.

521

522 **Synthesis of poly(2-vinyl-4,4'-dimethylazlactone) (PVDMA).** VDMA was passed through a
523 phenolic inhibitor removal resin followed by passage through a short plug of silica gel prior to
524 polymerization. The initiator 2,2'-azobisisobutyronitrile (AIBN) was recrystallized twice from
525 methanol prior to use. AIBN (5.9 mg, 0.036 mmol, 0.5 equiv.) and CTA (26 mg, 0.072 mmol, 1
526 equiv.) was weighed into a 25 mL schlenk-flask equipped with a stir bar. Anhydrous toluene (4.5
527 mL) was added to the flask and the mixture was stirred to dissolve the AIBN. VDMA (1.5 g, 10.8
528 mmol, 150 equiv.) was added to the flask, the flask was capped with a septum and placed in a dry
529 ice and isopropanol bath at ~7 torr. Atmosphere was purged from the flask using three freeze-
530 pump-thaw cycles and filled with nitrogen. The reaction solution was stirred at 70 °C for 12 h
531 (~85% conversion). The slightly viscous reaction mixture was cooled to room temperature and
532 acetone (~3 mL) was added to the flask. The polymer was precipitated twice into hexanes to yield
533 a pale yellow solid (1.26 g, 92% yield). ¹H-NMR (500 MHz, CDCl₃): δ = 1.37 (br s, (-CH₃)), 1.62-
534 2.1 (br m, -CH₂CH-), 2.69 (br s, -CH₂CH-). FT-IR (ATR, cm⁻¹): 2980-2900 (C-H), 1820 (lactone
535 C=O), 1672 (C=N). GPC: M_n = 13.1 kg/mol; PDI = 1.35.

536

537 **Synthesis of PVDMA-mTEG.** PVDMA (100 mg, 0.72 mmol with respect to the molecular weight
538 of the repeat unit VDMA) and mTEG (35 mg, 0.216 mmol, 0.3 equiv.) were combined in a 5 mL
539 round-bottomed flask and dissolved in anhydrous THF (3 mL). DBU (16.1 μL, 0.108 mmol, 0.15

540 equiv.) was added to catalyze the reaction. 4-Iodoanisole (50.5 mg, 0.216 mmol, 0.3 equiv) was
541 added as an internal standard for determining degree of functionalization. The flask was capped
542 with a rubber septum and purged with nitrogen for 15 minutes. The reaction was stirred at 40 °C
543 for 10 h. Prior to purification, an aliquot (~0.2 mL) of the reaction mixture was removed for ¹H
544 NMR analysis to determine the degree of mTEG functionalization. The remaining polymer
545 solution was purified by precipitation into diethyl ether (100 mL) followed by centrifugation
546 (9,000xg at 4°C, 2 min) to yield a yellow product. ¹H-NMR (300 MHz, CDCl₃): δ = 1.37-1.50 (br
547 m, (-CH₃)₂), 1.62-2.1 (br m, -CH₂CH-), 2.5 (br s, -CH₂CH-), 2.84 (br s, -CH₂CH-), 3.38 (br s, CH₃-
548 O-), 3.45-3.65 (br m, -CH₂-O-), 4.22 (br s, -C(=O)O-CH₂). FT-IR (ATR, cm⁻¹): 2880-2900 (C-H),
549 1820 (lactone C=O), 1735 (ester C=O), 1672 (C=N), 1650 (amide C=O), 1540 (amide II CN and
550 NH).

551
552 *PVDMA_{rc}-mTEG*. PVDMA-mTEG (50 mg, 0.26 mmol relative to the repeat unit) was dissolved in
553 anhydrous DMSO (1 mL) in a 1.5 mL microcentrifuge tube. Fluorescein cadaverine (FC) (0.95
554 mg, 1.3 μmol) was dissolved in anhydrous DMSO (9.5 μL) and added to the polymer solution.
555 The reaction was mixed by gentle rotation for 2 h at room temperature. The labeled polymer was
556 used for protein conjugation or hydrolysis without additional purification.

557
558 *Hydrolyzed PVDMA_{rc}-mTEG*. Unreactive, hydrolyzed PVDMA_{rc}-mTEG used for control
559 experiments was synthesized by dissolving PVDMA_{rc}-mTEG (100 mg) in DMSO (2 mL) in a 5
560 mL round bottom flask. Water (95.7 mg, 5.32 mmol, 10 eq relative to the azlactone repeat unit)
561 and DBU (202 mg, 1.33 mmol, 2.5 eq relative to the azlactone repeat unit) was added and the
562 solution was allowed to react at 40 °C for 3 h. Complete hydrolysis was confirmed using ATR-
563 FTIR spectroscopy. Samples were then dialyzed against PBS for 24 h (MWCO = 3.5 kDa) to
564 remove any small molecule impurities, including unreacted fluorophore, prior to incubation with
565 cells. FT-IR (ATR, cm⁻¹): 3500-2600 (O-H), 2880-2900 (C-H), 1725 (carboxylic acid C=O), 1650
566 (amide C=O), 1540 (amide II CN and NH).

567
568 *PVDMA-mTEG Hydrolysis Study*. PVDMA-mTEG (244 mg, 1.32 mmol relative to the repeat
569 unit) was dissolved in anhydrous DMSO (4.9 mL). PBS (11 mL) was added to simulate the
570 concentration of polymer used in a 1:50 molar ratio conjugation of hTF to polymer. At each time

571 point (0.5, 1, 3, 5, 9, 12, 24, 36 hours), a 1 mL sample (15.3 mg of polymer) was flash frozen in
572 liquid nitrogen and freeze dried. The samples were dissolved in acetone and cast directly onto the
573 ATR crystal for analysis by FT-IR spectroscopy.

574
575 ***Synthesis of Protein-polymer Conjugates.*** Proteins (i.e., hTF and OTF) were conjugated to
576 polymer using the following general procedure. Protein stock solutions of 1 mg/ml were prepared
577 in PBS with 0.1 M sodium bicarbonate (pH = 8.0), to increase the reactivity of the primary amines
578 of the protein. Polymer samples (i.e., PVDMA-mTEG or PVDMA_{ac}-mTEG) (50 mg) were
579 dissolved in DMSO (1 mL) in a microcentrifuge tube. A 1 ml aliquot of the desired protein (1 mg)
580 was added to polymer solution to achieve a protein:polymer molar ratio of 1:50, where a mole of
581 polymer was calculated using data from GPC analysis. The molecular weight of a monomer of
582 VDMA is 139 g/mol. Therefore, a molar ratio of 1 mol protein: 50 mol polymer is equivalent to
583 a molar ratio of 1 mol protein: 241 mol VDMA monomer. For studies examining the effect on
584 conjugation of the molar ratio of protein:polymer molecules, ratios of 1:5, 1:10, 1:20, and 1:50
585 were compared. The samples were reacted at 4 °C with gentle rotation overnight. Samples were
586 then dialyzed against PBS for 24 h (MWCO = 3.5 kDa) to remove any small molecule impurities,
587 including unreacted fluorophore, if the sample was not being purified by SEC.

588
589 ***Analysis of Protein-polymer Conjugates by SDS-PAGE.*** Sodium dodecyl sulfate-polyacrylamide
590 gel electrophoresis (SDS-PAGE) was used to analyze conjugation of protein to polymers.
591 NuPAGE LDS buffer (4X) was added to each sample to a final concentration of 1X, without
592 reducing agent. All proteins studied contain disulfide bonds, and therefore the absence of reducing
593 agents can shift their apparent molecular weight from the predicted molecular weight. The samples
594 were heated in a water bath for 10 min at 70 °C to denature the proteins. Samples were loaded onto
595 a NuPAGE 4-12% Bis-Tris gel. The gel was run in NuPAGE MES running buffer (1X). Gels were
596 then stained with Simply Blue Safe Stain.

597
598 ***Protein-polymer Conjugate Purification.*** Protein-polymer conjugation reactions were first
599 concentrated and purified from low molecular weight species using a centrifugal filtration device
600 with a MWCO of 10 kDa (EMD Millipore) and extensive washing with PBS. The protein-polymer
601 conjugation reaction was then purified by SEC on a Superdex 75 10/300 column (GE Healthcare

602 Life Sciences). Fractions of interest were pooled and concentrated with a centrifugal filtration
603 device with a 10 kDa MWCO. All samples were analyzed by SDS-PAGE and imaged on a BioRad
604 ChemiDoc MP imaging system using Image Lab 6.0 software (BioRad).

605

606 ***Cells, Cell Culture, and Receptor Detection.*** The MCF-7 human breast cancer cell line (ATCC
607 #HTB-22, acquired in 2018) was used to test internalization of protein-polymer conjugates via
608 receptor-mediated endocytosis of TFR. MCF-7 cells were cultured at 37 °C in a humidified
609 atmosphere with 5% CO₂ in DMEM with 10% fetal bovine serum, 100 U/ml penicillin, and 100
610 µg/ml streptomycin. Cells were subcultured after reaching 80% confluency using 0.25% trypsin-
611 EDTA. The presence of human TFR on the surface of MCF-7 cells was confirmed with an anti-
612 human TFR antibody directly labeled with fluorescein isothiocyanate (antibody clone CY1G4,
613 from BioLegend, Cat.: 334103). MCF-7 cells were harvested with 0.05% trypsin-EDTA. 1 x 10⁶
614 cells were incubated with antibody at a 1:20 dilution in PBS with 0.1% bovine serum albumin
615 (PBSA) for 30 min at room temperature with gentle rotation. Cells were washed with PBSA to
616 remove unbound antibody, resuspended in PBSA, and analyzed by flow cytometry.

617

618 ***Internalization Assays and Confocal Microscopy.*** MCF-7 cells were seeded in a 4-well Millipore
619 EZ chamber slide using 4x10⁴ cells/well and allowed to establish adherence and reach 50-80%
620 confluency. The media was then replaced with serum-free DMEM containing the specified
621 conjugate sample in a 500 µl total volume. hTF-488, hTF-PVDMA_{rc}-mTEG, OTF-488, or OTF-
622 PVDMA_{rc}-mTEG were added to the wells to a final concentration equivalent to 10 nM of protein
623 per well. For the internalization sample with hydrolyzed PVDMA_{rc} that was not conjugated to
624 protein, an amount of polymer equivalent to the amount of polymer in 10 nM of protein-polymer
625 conjugate was used, as determined by measurement of samples by UV-vis spectroscopy, using
626 absorbance at 494 nm due to the presence of fluorophore. For competition experiments with
627 unlabeled hTF, 10 µM unlabeled hTF was included. For the competition experiment with excess
628 unlabeled polymer, 0.5 mg of hydrolyzed PVDMA-mTEG was included. Samples were incubated
629 for 1 h at 37 °C in a humidified environment with 5% CO₂. Media with samples were removed,
630 and cells were washed with PBS. Cells were fixed with 3.7% formaldehyde for 5-10 minutes at
631 room temperature, and washed with PBS. Cells were permeabilized by incubation with 0.1%
632 Triton-X 100 in PBS at room temperature for 5 min, and washed with PBS. Actin filaments were

633 stained with an Alexa Fluor 594 conjugate of phalloidin to help identify cell boundaries by adding
634 250 μ l per well of phalloidin in PBS diluted following manufacturer's protocol, and cells were
635 washed with PBS. Wells were removed from the slide and Vectashield mounting media containing
636 DAPI for staining cell nuclei was applied to the fixed samples. Samples were then covered with
637 1.5 mm glass coverslips and sealed with transparent nail polish. Samples were imaged using a 63X
638 oil immersion objective. Images were collected using sequential scanning, and an overlay of the
639 sequential images was used to analyze internalization, for single focal plane images and for z-
640 stacks collected as a series of neighboring focal planes.

641

642 **ASSOCIATED CONTENT**

643

644 **Supporting Information**

645 Supporting experimental procedures as well as supporting figures and videos related to: SEC and
646 UV-Vis spectroscopy analysis of PVDMA-mTEG; TFR expression and hTF binding to MCF-7
647 cells; hTF-488 internalization into MCF-7 cells is concentration dependent (PDF). Internalization
648 of hTF-488 and hTF-PVDMA_{FC}-mTEG into cells visualized by z-stack series videos (.avi files).

649

650 **AUTHOR INFORMATION**

651

652 ***Corresponding Authors**

653 E-mail: mbuck@smith.edu

654 E-mail: sjmoore@smith.edu

655

656 **ORCID**

657 Allison R. Sirois: 0000-0001-7807-6927

658 Maren E. Buck: 0000-0002-1404-8588

659 Sarah J. Moore: 0000-0002-2633-4020

660

661 **NOTES**

662 #Author Contributions

663 J. S. K., A. R. S., and A. J. V. C. contributed equally to this work.

664 The authors declare no competing financial interests.

665

666 **ACKNOWLEDGMENTS**

667

668 This work was funded by Smith College new faculty funding to S.J.M. and to M.E.B. J.S.K.
669 received a Katherine C. Hauch 1921 Fund Undergraduate Research Fellowship and A.V.C.
670 received a Schultz Foundation Undergraduate Research Fellowship. J.S.K., A.V.C., and E.J.
671 received support from the Nancy Kershaw Tomlinson Memorial Fund at Smith College. This
672 work was supported by the National Institutes of Health/National Cancer Institute (R15CA198927-
673 01 to S.J.M). We thank Lou Ann Bierwert, Director for the Smith College Center for Molecular
674 Biology; Judith Wopereis, Director for the Smith College Center for Microscopy and Imaging;
675 and Kalina Dimova, Technical Director of the Smith College Center for Proteomics for expert
676 insight and technical assistance. We thank Krystal Cogar and Stephen Rosa in the Department of
677 Polymer Science and Engineering at the University of Massachusetts Amherst for running all GPC
678 samples. We acknowledge Anne Mason at the University of Vermont for insightful discussions,
679 and Michael Kinsinger at Smith College and Patrick Flaherty at the University of Massachusetts
680 for helpful discussions and critical reading of the manuscript.

681

682 **ABBREVIATIONS**

683

684 AIBN, 2,2'-azobis(2-methylpropionitrile); BBB, blood-brain barrier; FC, fluoresceine cadaverine;
685 hTF, holo-transferrin; hTF-488, holo-transferrin labeled with Alexa Fluor 488; mTEG, triethylene
686 glycol monomethyl ether; MWCO, molecular weight cut-off; OTF, ovotransferrin; OTF-488,
687 ovotransferrin labeled with Alexa Fluor 488; PEG, polyethylene glycol; PVDMA, poly(2-vinyl-
688 4,4-dimethylazlactone); RAFT, reversible addition-fragmentation transfer; RMT, receptor-
689 mediated transcytosis; TFR, transferrin receptor; VDMA, 2-vinyl-4,4-dimethylazlactone.

690

691 **REFERENCES**

692

693 (1) Chen, Y.; Liu, L. Modern Methods for Delivery of Drugs across the Blood–Brain Barrier.
694 *Adv. Drug Deliv. Rev.* 2012, 64 (7), 640–665. <https://doi.org/10.1016/j.addr.2011.11.010>.

- 695 (2) Patel, M. M.; Patel, B. M. Crossing the Blood–Brain Barrier: Recent Advances in Drug
696 Delivery to the Brain. *CNS Drugs* 2017, *31* (2), 109–133. [https://doi.org/10.1007/s40263-016-](https://doi.org/10.1007/s40263-016-0405-9)
697 0405-9.
- 698 (3) Mikitsh, J. L.; Chacko, A.-M. Pathways for Small Molecule Delivery to the Central
699 Nervous System across the Blood-Brain Barrier. *Perspect. Med. Chem.* 2014, *6*, PMC.S13384.
700 <https://doi.org/10.4137/PMC.S13384>.
- 701 (4) Lajoie, J. M.; Shusta, E. V. Targeting Receptor-Mediated Transport for Delivery of
702 Biologics Across the Blood-Brain Barrier. *Annu. Rev. Pharmacol. Toxicol.* 2015, *55* (1), 613–631.
703 <https://doi.org/10.1146/annurev-pharmtox-010814-124852>.
- 704 (5) Pardridge, W. M.; Boado, R. J. Reengineering Biopharmaceuticals for Targeted Delivery
705 Across the Blood–Brain Barrier. In *Methods in Enzymology*; Elsevier, 2012; Vol. 503, pp 269–
706 292. <https://doi.org/10.1016/B978-0-12-396962-0.00011-2>.
- 707 (6) Giugliani, R.; Giugliani, L.; Corte, A. D.; Poswar, F.; Donis, K.; Schmidt, M.; Hunt, D.;
708 Boado, R. J.; Pardridge, W. M. Safety and Clinical Efficacy of AGT-181, a Brain Penetrating
709 Human Insulin Receptor Antibody-Iduronidase Fusion Protein, in a 26-Week Study with Pediatric
710 Patients with Mucopolysaccharidosis Type I. *Mol. Genet. Metab.* 2018, *123* (2), S54.
711 <https://doi.org/10.1016/j.ymgme.2017.12.128>.
- 712 (7) Bae, Y. H.; Park, K. Targeted Drug Delivery to Tumors: Myths, Reality and Possibility. *J.*
713 *Controlled Release* 2011, *153* (3), 198–205. <https://doi.org/10.1016/j.jconrel.2011.06.001>.
- 714 (8) Gordon, M. R.; Canakci, M.; Li, L.; Zhuang, J.; Osborne, B.; Thayumanavan, S. Field
715 Guide to Challenges and Opportunities in Antibody–Drug Conjugates for Chemists. *Bioconjug.*
716 *Chem.* 2015, *26* (11), 2198–2215. <https://doi.org/10.1021/acs.bioconjchem.5b00399>.
- 717 (9) Perez, H. L.; Cardarelli, P. M.; Deshpande, S.; Gangwar, S.; Schroeder, G. M.; Vite, G. D.;
718 Borzilleri, R. M. Antibody–Drug Conjugates: Current Status and Future Directions. *Drug Discov.*
719 *Today* 2014, *19* (7), 869–881. <https://doi.org/10.1016/j.drudis.2013.11.004>.
- 720 (10) Nirnoy Dan; Saini Setua; Vivek Kashyap; Sheema Khan; Meena Jaggi; Murali Yallapu;
721 Subhash Chauhan. Antibody-Drug Conjugates for Cancer Therapy: Chemistry to Clinical
722 Implications. *Pharmaceuticals* 2018, *11* (2), 32. <https://doi.org/10.3390/ph11020032>.
- 723 (11) Bobo, D.; Robinson, K. J.; Islam, J.; Thurecht, K. J.; Corrie, S. R. Nanoparticle-Based
724 Medicines: A Review of FDA-Approved Materials and Clinical Trials to Date. *Pharm. Res.* 2016,
725 *33* (10), 2373–2387. <https://doi.org/10.1007/s11095-016-1958-5>.

- 726 (12) Rosenblum, D.; Joshi, N.; Tao, W.; Karp, J. M.; Peer, D. Progress and Challenges towards
727 Targeted Delivery of Cancer Therapeutics. *Nat. Commun.* 2018, 9 (1), 1410.
728 <https://doi.org/10.1038/s41467-018-03705-y>.
- 729 (13) Carter, P. J. Introduction to Current and Future Protein Therapeutics: A Protein
730 Engineering Perspective. *Exp. Cell Res.* 2011, 317 (9), 1261–1269.
731 <https://doi.org/10.1016/j.yexcr.2011.02.013>.
- 732 (14) Kariolis, M. S.; Kapur, S.; Cochran, J. R. Beyond Antibodies: Using Biological Principles
733 to Guide the Development of next-Generation Protein Therapeutics. *Curr. Opin. Biotechnol.* 2013,
734 24 (6), 1072–1077. <https://doi.org/10.1016/j.copbio.2013.03.017>.
- 735 (15) Kinch, M. S. An Overview of FDA-Approved Biologics Medicines. *Drug Discov. Today*
736 2015, 20 (4), 393–398. <https://doi.org/10.1016/j.drudis.2014.09.003>.
- 737 (16) Rodgers, K. R.; Chou, R. C. Therapeutic Monoclonal Antibodies and Derivatives:
738 Historical Perspectives and Future Directions. *Biotechnol. Adv.* 2016, 34 (6), 1149–1158.
739 <https://doi.org/10.1016/j.biotechadv.2016.07.004>.
- 740 (17) Qi, Y.; Chilkoti, A. Protein–Polymer Conjugation—Moving beyond PEGylation. *Curr.*
741 *Opin. Chem. Biol.* 2015, 28, 181–193. <https://doi.org/10.1016/j.cbpa.2015.08.009>.
- 742 (18) Pelegri-O’Day, E. M.; Lin, E.-W.; Maynard, H. D. Therapeutic Protein–Polymer
743 Conjugates: Advancing Beyond PEGylation. *J. Am. Chem. Soc.* 2014, 136 (41), 14323–14332.
744 <https://doi.org/10.1021/ja504390x>.
- 745 (19) Russell, A. J.; Baker, S. L.; Colina, C. M.; Figg, C. A.; Kaar, J. L.; Matyjaszewski, K.;
746 Simakova, A.; Sumerlin, B. S. Next Generation Protein-Polymer Conjugates. *AIChE J.* 2018.
747 <https://doi.org/10.1002/aic.16338>.
- 748 (20) Pasut, G.; Veronese, F. M. State of the Art in PEGylation: The Great Versatility Achieved
749 after Forty Years of Research. *J. Controlled Release* 2012, 161 (2), 461–472.
750 <https://doi.org/10.1016/j.jconrel.2011.10.037>.
- 751 (21) Alconcel, S. N. S.; Baas, A. S.; Maynard, H. D. FDA-Approved Poly(Ethylene Glycol)–
752 Protein Conjugate Drugs. *Polym. Chem.* 2011, 2 (7), 1442. <https://doi.org/10.1039/c1py00034a>.
- 753 (22) Jevšičevar, S.; Kunstelj, M.; Porekar, V. G. PEGylation of Therapeutic Proteins.
754 *Biotechnol. J.* 2010, 5 (1), 113–128. <https://doi.org/10.1002/biot.200900218>.

- 755 (23) Schellekens, H.; Hennink, W. E.; Brinks, V. The Immunogenicity of Polyethylene Glycol:
756 Facts and Fiction. *Pharm. Res.* 2013, *30* (7), 1729–1734. [https://doi.org/10.1007/s11095-013-](https://doi.org/10.1007/s11095-013-1067-7)
757 1067-7.
- 758 (24) Zhao, W.; Liu, F.; Chen, Y.; Bai, J.; Gao, W. Synthesis of Well-Defined Protein–Polymer
759 Conjugates for Biomedicine. *Polymer* 2015, *66*, A1–A10.
760 <https://doi.org/10.1016/j.polymer.2015.03.054>.
- 761 (25) Broyer, R. M.; Grover, G. N.; Maynard, H. D. Emerging Synthetic Approaches for Protein–
762 Polymer Conjugations. *Chem. Commun.* 2011, *47* (8), 2212. <https://doi.org/10.1039/c0cc04062b>.
- 763 (26) Pelegri-O’Day, E. M.; Maynard, H. D. Controlled Radical Polymerization as an Enabling
764 Approach for the Next Generation of Protein–Polymer Conjugates. *Acc. Chem. Res.* 2016, *49* (9),
765 1777–1785. <https://doi.org/10.1021/acs.accounts.6b00258>.
- 766 (27) Baslé, E.; Joubert, N.; Pucheault, M. Protein Chemical Modification on Endogenous
767 Amino Acids. *Chem. Biol.* 2010, *17* (3), 213–227. <https://doi.org/10.1016/j.chembiol.2010.02.008>.
- 768 (28) Cobo, I.; Li, M.; Sumerlin, B. S.; Perrier, S. Smart Hybrid Materials by Conjugation of
769 Responsive Polymers to Biomacromolecules. *Nat. Mater.* 2015, *14* (2), 143–159.
770 <https://doi.org/10.1038/nmat4106>.
- 771 (29) Murata, H.; Carmali, S.; Baker, S. L.; Matyjaszewski, K.; Russell, A. J. Solid-Phase
772 Synthesis of Protein-Polymers on Reversible Immobilization Supports. *Nat. Commun.* 2018, *9* (1).
773 <https://doi.org/10.1038/s41467-018-03153-8>.
- 774 (30) Plaks, J. G.; Falatach, R.; Kastantin, M.; Berberich, J. A.; Kaar, J. L. Multisite Clickable
775 Modification of Proteins Using Lipoic Acid Ligase. *Bioconjug. Chem.* 2015, *26* (6), 1104–1112.
776 <https://doi.org/10.1021/acs.bioconjchem.5b00161>.
- 777 (31) Qi, Y.; Amiram, M.; Gao, W.; McCafferty, D. G.; Chilkoti, A. Sortase-Catalyzed Initiator
778 Attachment Enables High Yield Growth of a Stealth Polymer from the C Terminus of a Protein.
779 *Macromol. Rapid Commun.* 2013, *34* (15), 1256–1260. <https://doi.org/10.1002/marc.201300460>.
- 780 (32) Krall, N.; da Cruz, F. P.; Boutureira, O.; Bernardes, G. J. L. Site-Selective Protein-
781 Modification Chemistry for Basic Biology and Drug Development. *Nat. Chem.* 2016, *8* (2), 103–
782 113. <https://doi.org/10.1038/nchem.2393>.
- 783 (33) Peeler, J. C.; Woodman, B. F.; Averick, S.; Miyake-Stoner, S. J.; Stokes, A. L.; Hess, K.
784 R.; Matyjaszewski, K.; Mehl, R. A. Genetically Encoded Initiator for Polymer Growth from
785 Proteins. *J. Am. Chem. Soc.* 2010, *132* (39), 13575–13577. <https://doi.org/10.1021/ja104493d>.

- 786 (34) Wang, Y.; Wu, C. Site-Specific Conjugation of Polymers to Proteins. *Biomacromolecules*
787 2018, *19* (6), 1804–1825. <https://doi.org/10.1021/acs.biomac.8b00248>.
- 788 (35) Le Droumaguet, B.; Nicolas, J. Recent Advances in the Design of Bioconjugates from
789 Controlled/Living Radical Polymerization. *Polym. Chem.* 2010, *1* (5), 563.
790 <https://doi.org/10.1039/b9py00363k>.
- 791 (36) Paeth, M.; Stapleton, J.; Dougherty, M. L.; Fischesser, H.; Shepherd, J.; McCauley, M.;
792 Falatach, R.; Page, R. C.; Berberich, J. A.; Konkolewicz, D. Approaches for Conjugating Tailor-
793 Made Polymers to Proteins. In *Methods in Enzymology*; Elsevier, 2017; Vol. 590, pp 193–224.
794 <https://doi.org/10.1016/bs.mie.2016.12.004>.
- 795 (37) Isarov, S. A.; Lee, P. W.; Pokorski, J. K. “Graft-to” Protein/Polymer Conjugates Using
796 Polynorbornene Block Copolymers. *Biomacromolecules* 2016, *17* (2), 641–648.
797 <https://doi.org/10.1021/acs.biomac.5b01582>.
- 798 (38) Jones, M. W.; Strickland, R. A.; Schumacher, F. F.; Caddick, S.; Baker, J. R.; Gibson, M.
799 I.; Haddleton, D. M. Polymeric Dibromomaleimides As Extremely Efficient Disulfide Bridging
800 Bioconjugation and Pegylation Agents. *J. Am. Chem. Soc.* 2012, *134* (3), 1847–1852.
801 <https://doi.org/10.1021/ja210335f>.
- 802 (39) Hall, D. J.; Van den Berghe, H. M.; Dove, A. P. Synthesis and Post-Polymerization
803 Modification of Maleimide-Containing Polymers by “thiol-Ene” Click and Diels-Alder
804 Chemistries. *Polym. Int.* 2011, *60* (8), 1149–1157. <https://doi.org/10.1002/pi.3121>.
- 805 (40) Alvaradejo, G. G.; Glassner, M.; Hoogenboom, R.; Delaittre, G. Maleimide End-
806 Functionalized Poly(2-Oxazoline)s by the Functional Initiator Route: Synthesis and (Bio)
807 Conjugation. *Rsc Adv.* 2018, *8* (17), 9471–9479. <https://doi.org/10.1039/c8ra00948a>.
- 808 (41) Moatsou, D.; Li, J.; Ranji, A.; Pitto-Barry, A.; Ntai, I.; Jewett, M. C.; O’Reilly, R. K. Self-
809 Assembly of Temperature-Responsive Protein–Polymer Bioconjugates. *Bioconjug. Chem.* 2015,
810 *26* (9), 1890–1899. <https://doi.org/10.1021/acs.bioconjchem.5b00264>.
- 811 (42) Das, A.; Theato, P. Activated Ester Containing Polymers: Opportunities and Challenges
812 for the Design of Functional Macromolecules. *Chem. Rev.* 2016, *116* (3), 1434–1495.
813 <https://doi.org/10.1021/acs.chemrev.5b00291>.
- 814 (43) W. Jones, M.; Richards, S.-J.; M. Haddleton, D.; I. Gibson, M. Poly(Azlactone)s: Versatile
815 Scaffolds for Tandem Post-Polymerisation Modification and Glycopolymer Synthesis. *Polym.*
816 *Chem.* 2013, *4* (3), 717–723. <https://doi.org/10.1039/C2PY20757E>.

817 (44) Gauthier, M. A.; Gibson, M. I.; Klok, H.-A. Synthesis of Functional Polymers by Post-
818 Polymerization Modification. *Angew. Chem. Int. Ed.* 48 (1), 48–58.
819 <https://doi.org/10.1002/anie.200801951>.

820 (45) Buck, M. E.; Lynn, D. M. Azlactone -Functionalized Polymers as Reactive Platforms for
821 the Design of Advanced Materials: Progress in the Last Ten Years. *Polym. Chem.* 2012, 3 (1), 66–
822 80. <https://doi.org/10.1039/C1PY00314C>.

823 (46) Zhong, Y.; Zeberl, B. J.; Wang, X.; Luo, J. Combinatorial Approaches in Post-
824 Polymerization Modification for Rational Development of Therapeutic Delivery Systems. *Acta*
825 *Biomater.* 2018, 73, 21–37. <https://doi.org/10.1016/j.actbio.2018.04.010>.

826 (47) Ho, H. T.; Levere, M. E.; Fournier, D.; Montembault, V.; Pascual, S.; Fontaine, L.
827 Introducing the Azlactone Functionality into Polymers through Controlled Radical
828 Polymerization: Strategies and Recent Developments. *Aust. J. Chem.* 2012, 65 (8), 970–977.
829 <https://doi.org/10.1071/CH12192>.

830 (48) Ho, H. T.; Levere, M. E.; Pascual, S.; Montembault, V.; Casse, N.; Caruso, A.; Fontaine,
831 L. Thermoresponsive Block Copolymers Containing Reactive Azlactone Groups and Their
832 Bioconjugation with Lysozyme. *Polym. Chem.* 2013, 4 (3), 675–685.
833 <https://doi.org/10.1039/C2PY20714A>.

834 (49) Pascual, S.; Blin, T.; Saikia, P. J.; Thomas, M.; Gosselin, P.; Fontaine, L. Block
835 Copolymers Based on 2-Vinyl-4,4-Dimethyl-5-Oxazolone by RAFT Polymerization:
836 Experimental and Computational Studies. *J. Polym. Sci. Part Polym. Chem.* 2010, 48 (22), 5053–
837 5062. <https://doi.org/10.1002/pola.24303>.

838 (50) Speetjens, F. W.; Carter, M. C. D.; Kim, M.; Gopalan, P.; Mahanthappa, M. K.; Lynn, D.
839 M. Post-Fabrication Placement of Arbitrary Chemical Functionality on Microphase-Separated
840 Thin Films of Amine-Reactive Block Copolymers. *ACS Macro Lett.* 2014, 3 (11), 1178–1182.
841 <https://doi.org/10.1021/mz500654a>.

842 (51) Heilmann, S. M.; Rasmussen, J. K.; Krepski, L. R. Chemistry and Technology of 2-Alkenyl
843 Azlactones. *J. Polym. Sci. Part Polym. Chem.* 2001, 39 (21), 3655–3677.
844 <https://doi.org/10.1002/pola.10007>.

845 (52) Delplace, V.; Harriison, S.; Ho, H. T.; Tardy, A.; Guillaneuf, Y.; Pascual, S.; Fontaine, L.;
846 Nicolas, J. One-Step Synthesis of Azlactone-Functionalized SG1-Based Alkoxyamine for

847 Nitroxide-Mediated Polymerization and Bioconjugation. *Macromolecules* 2015, 48 (7), 2087–
848 2097. <https://doi.org/10.1021/acs.macromol.5b00178>.

849 (53) Weeks, C. A.; Aden, B.; Kilbey, S. M.; Janorkar, A. V. Synthesis and Characterization of
850 an Array of Elastin-like Polypeptide–Polyelectrolyte Conjugates with Varying Chemistries and
851 Amine Content for Biomedical Applications. *ACS Biomater. Sci. Eng.* 2016, 2 (12), 2196–2206.
852 <https://doi.org/10.1021/acsbiomaterials.6b00398>.

853 (54) Gardner, C. M.; Brown, C. E.; Stöver, H. D. H. Synthesis and Properties of Water-Soluble
854 Azlactone Copolymers. *J. Polym. Sci. Part Polym. Chem.* 50 (22), 4674–4685.
855 <https://doi.org/10.1002/pola.26281>.

856 (55) Zhu, Y.; Quek, J. Y.; Lowe, A. B.; Roth, P. J. Thermoresponsive (Co)Polymers through
857 Postpolymerization Modification of Poly(2-Vinyl-4,4-Dimethylazlactone). *Macromolecules*
858 2013, 46 (16), 6475–6484. <https://doi.org/10.1021/ma401096r>.

859 (56) Luck, A. N.; Mason, A. B. Structure and Dynamics of Drug Carriers and Their Interaction
860 with Cellular Receptors: Focus on Serum Transferrin. *Adv. Drug Deliv. Rev.* 2013, 65 (8), 1012–
861 1019. <https://doi.org/10.1016/j.addr.2012.11.001>.

862 (57) Wong, A. S. M.; Czuba, E.; Chen, M. Z.; Yuen, D.; Cupic, K. I.; Yang, S.; Hodgetts, R.
863 Y.; Selby, L. I.; Johnston, A. P. R.; Such, G. K. PH-Responsive Transferrin-PHlexi Particles
864 Capable of Targeting Cells *in Vitro*. *ACS Macro Lett.* 2017, 6 (3), 315–320.
865 <https://doi.org/10.1021/acsmacrolett.7b00044>.

866 (58) Carter, M. C. D.; Jennings, J.; Speetjens, F. W.; Lynn, D. M.; Mahanthappa, M. K. A
867 Reactive Platform Approach for the Rapid Synthesis and Discovery of High χ /Low N Block
868 Polymers. *Macromolecules* 2016, 49 (17), 6268–6276.
869 <https://doi.org/10.1021/acs.macromol.6b01268>.

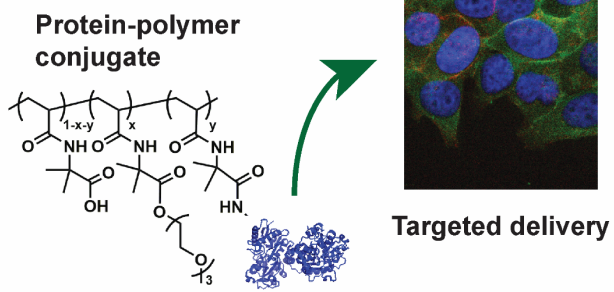
870 (59) Paterson, J.; Webster, C. I. Exploiting Transferrin Receptor for Delivering Drugs across
871 the Blood-Brain Barrier. *Drug Discov. Today Technol.* 2016, 20, 49–52.
872 <https://doi.org/10.1016/j.ddtec.2016.07.009>.

873 (60) Daniels, T. R.; Bernabeu, E.; Rodríguez, J. A.; Patel, S.; Kozman, M.; Chiappetta, D. A.;
874 Holler, E.; Ljubimova, J. Y.; Helguera, G.; Penichet, M. L. The Transferrin Receptor and the
875 Targeted Delivery of Therapeutic Agents against Cancer. *Biochim. Biophys. Acta BBA - Gen. Subj.*
876 2012, 1820 (3), 291–317. <https://doi.org/10.1016/j.bbagen.2011.07.016>.

- 877 (61) Jiang, Y.; Liang, M.; Svejkar, D.; Hart-Smith, G.; Lu, H.; Scarano, W.; Stenzel, M. H.
878 Albumin-Micelles via a One-Pot Technology Platform for the Delivery of Drugs. *Chem. Commun.*
879 2014, 50 (48), 6394–6397. <https://doi.org/10.1039/C4CC00616J>.
- 880 (62) Leverage, R.; Mason, A. B.; Kaltashov, I. A. Noncanonical Interactions between Serum
881 Transferrin and Transferrin Receptor Evaluated with Electrospray Ionization Mass Spectrometry.
882 *Proc. Natl. Acad. Sci.* 2010, 107 (18), 8123–8128. <https://doi.org/10.1073/pnas.0914898107>.
- 883 (63) Vandewalle, B.; Granier, A. M.; Peyrat, J. P.; Bonnetterre, J.; Lefebvre, J. Detection of
884 Transferrin Receptors in Cultured Breast Cancer Cells. *Ann. N. Y. Acad. Sci.* 1986, 464 (1
885 Endocrinology), 482–485. <https://doi.org/10.1111/j.1749-6632.1986.tb16042.x>.
- 886 (64) Tortorella, S.; Karagiannis, T. C. Transferrin Receptor-Mediated Endocytosis: A Useful
887 Target for Cancer Therapy. *J. Membr. Biol.* 2014, 247 (4), 291–307.
888 <https://doi.org/10.1007/s00232-014-9637-0>.
- 889 (65) Lim, C.-J.; Norouziyan, F.; Shen, W.-C. Accumulation of Transferrin in Caco-2 Cells: A
890 Possible Mechanism of Intestinal Transferrin Absorption. *J. Controlled Release* 2007, 122 (3),
891 393–398. <https://doi.org/10.1016/j.jconrel.2007.03.021>.
- 892 (66) Pardridge, W. Targeted Delivery of Protein and Gene Medicines through the Blood-Brain
893 Barrier. *Clin. Pharmacol. Ther.* 2015, 97 (4), 347–361. <https://doi.org/10.1002/cpt.18>.
- 894 (67) Goulatis, L. I.; Shusta, E. V. Protein Engineering Approaches for Regulating Blood–Brain
895 Barrier Transcytosis. *Curr. Opin. Struct. Biol.* 2017, 45, 109–115.
896 <https://doi.org/10.1016/j.sbi.2016.12.005>.
- 897 (68) Yu, Y. J.; Atwal, J. K.; Zhang, Y.; Tong, R. K.; Wildsmith, K. R.; Tan, C.; Bien-Ly, N.;
898 Hersom, M.; Maloney, J. A.; Meilandt, W. J.; et al. Therapeutic Bispecific Antibodies Cross the
899 Blood-Brain Barrier in Nonhuman Primates. *Sci. Transl. Med.* 2014, 6 (261), 261ra154-261ra154.
900 <https://doi.org/10.1126/scitranslmed.3009835>.
- 901 (69) Wancura, M. M.; Anex-Ries, Q.; Carroll, A. L.; Garcia, A. P.; Hindocha, P.; Buck, M. E.
902 Fabrication, Chemical Modification, and Topographical Patterning of Reactive Gels Assembled
903 from Azlactone-Functionalized Polymers and a Diamine. *J. Polym. Sci. Part Polym. Chem.* 2017,
904 55 (19), 3185–3194. <https://doi.org/10.1002/pola.28664>.

905

906 **FOR TABLE OF CONTENTS ONLY**



907

1 **SUPPORTING INFORMATION**

2
3 for

4
5 **Protein-Polymer Conjugates Synthesized using Water-Soluble Azlactone-Functionalized**
6 **Polymers Enable Receptor-Specific Cellular Uptake towards Targeted Drug Delivery**
7

8 Julia S. Kim^{*,§}, Allison R. Sirois^{§,¶}, Analia J. Vazquez Cegla^{§,¶}, Eugenie Jumai^{¶,an†}, Naomi Murata[‡],
9 Maren E. Buck^{*†}, and Sarah J. Moore^{*,‡,∇}

10
11 **AFFILIATIONS**

12 [¶]Biochemistry Program, [†]Picker Engineering Program, [‡]Neuroscience Program, [†]Department of
13 Chemistry, and [∇]Department of Biological Sciences, Smith College, Northampton, Massachusetts
14 01063, United States

15 [§]Molecular and Cellular Biology Program, University of Massachusetts Amherst, Amherst,
16 Massachusetts 01003, United States

17
18 *Corresponding Authors

19 Email: mbuck@smith.edu

20 Email: sjmoore@smith.edu

21
22 **TABLE OF CONTENTS**

23
24 Experimental procedures S2
25
26 Figure S1. PVDMA-mTEG analysis by size exclusion chromatography and UV-Vis
27 spectroscopy..... S4
28
29 Figure S2. MCF-7 cells express TFR and bind hTF S5
30
31 Figure S3. hTF-488 internalization into MCF-7 cells is concentration dependent S6
32
33 Description of supporting information videos.....S7

34 **EXPERIMENTAL PROCEDURES**

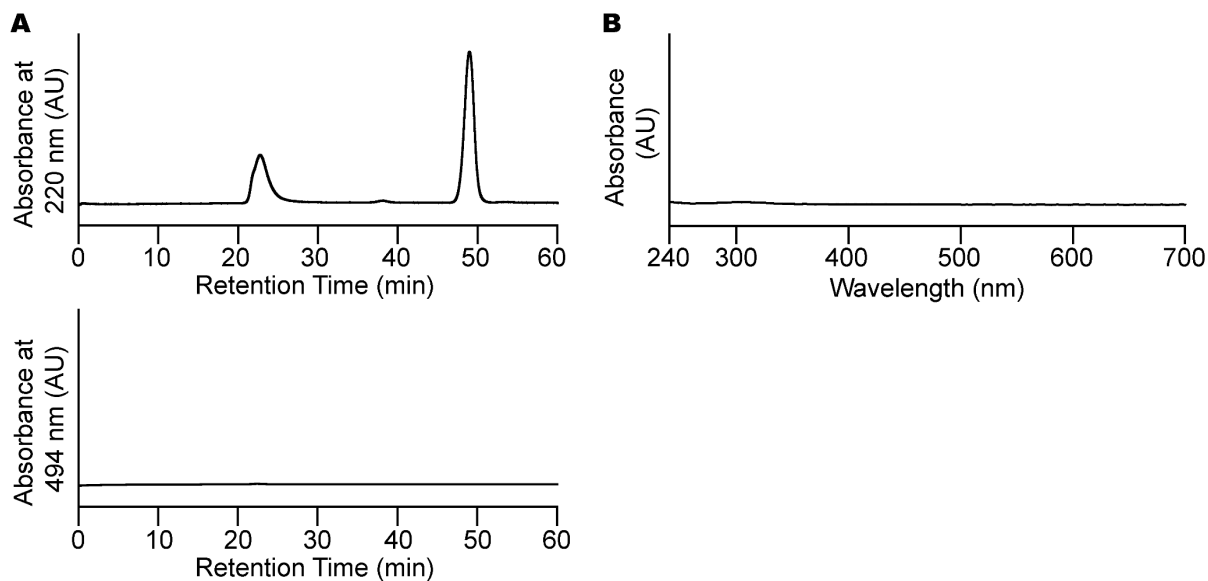
35 ***Labeling hTF and OTF with Alexa Fluor 488.*** Holo-transferrin (hTF) or ovotransferrin (OTF)
36 were labeled with Alexa Fluor 488 (AF488) by primary amine chemistry. A solution of protein
37 (1-2 mg/ml) was made in phosphate buffered saline (PBS). Sodium bicarbonate (1M stock
38 solution) was added to the protein to a final concentration of 0.1 M to change the pH of the solution
39 to 8.0. The fluorescent dye AF488 5-tetrafluorophenyl ester was dissolved in anhydrous DMSO to
40 a final concentration of 11.3 nM. Dye was added to protein solution, using an amount of dye
41 calculated following manufacturer's protocol to achieve a desired molar excess of dye. The sample
42 was incubated with gentle rotation at room temperature for 1 h. The protein labeled with AF488
43 was then purified from free dye and concentrated using an Amicon centrifugal filtration device
44 with a molecular weight cutoff of 10 kDa by washing extensively with PBS until the flow through
45 was colorless. Concentrations and degree of labeling were determined using UV-Vis spectroscopy,
46 measuring dye absorption at 494 nm ($\epsilon = 71,000 \text{ cm}^2 \text{ M}^{-1}$). Labeled protein was stored at 4 °C.

47

48 ***Titration Binding Assay of hTF-488 with MCF-7 Cells.*** Titration binding assays were performed
49 to experimentally determine the binding affinity (dissociation constant, K_d) of hTF with MCF-7
50 cells. MCF-7 cells were harvested with 0.05% trypsin-EDTA. Aliquots of 1×10^5 cells were
51 incubated for 1 h at 4 °C with a range of concentrations of fluorescently labeled hTF (hTF-488,
52 0.5-500 nM) in PBS with 0.1% BSA (PBSA) with gentle rotation. Following incubation to reach
53 equilibrium binding, cells were washed in PBSA and resuspended in PBSA for analysis. Data was
54 collected and analyzed using flow cytometry. Experimental triplicate data was collected to
55 determine the binding affinity of hTF to its receptor. For each replicate, the data were fit to a
56 sigmoidal binding curve using Kaleidagraph software (Synergy). The concentration of hTF-488

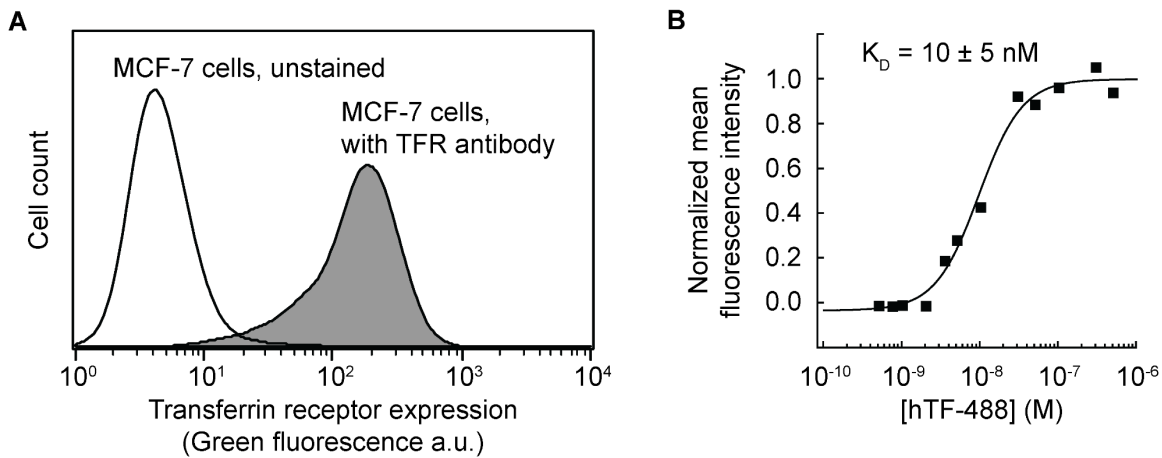
57 that resulted in the half-maximal value of each best-fit line was determined as the K_o . The mean
58 of the three individually fit dissociation constants was determined and reported with the standard
59 deviation.

60 **Figure S1**
61



62
63 **Figure S1. PVDMA-mTEG analysis by size exclusion chromatography and UV-Vis**
64 **spectroscopy.** (A) PVDMA functionalized with 0.3 molar equivalents of mTEG was analyzed on
65 a Superdex 75 30/100 SEC column run at 0.4 ml/min, and absorbance was detected at 220 nm and
66 at 494 nm. For absorbance at 220 nm, the functionalized polymer sample contains a broad peak
67 characteristic of polymers with a molecular weight distribution eluting between 20 and 30 minutes,
68 and a second peak of low molecular weight byproducts eluting around 50 minutes. There is no
69 absorbance at 494 nm. (B) PVDMA-mTEG analyzed using UV-Vis spectroscopy has no
70 absorbance in the 240-700 nm range, as expected for the polymer.

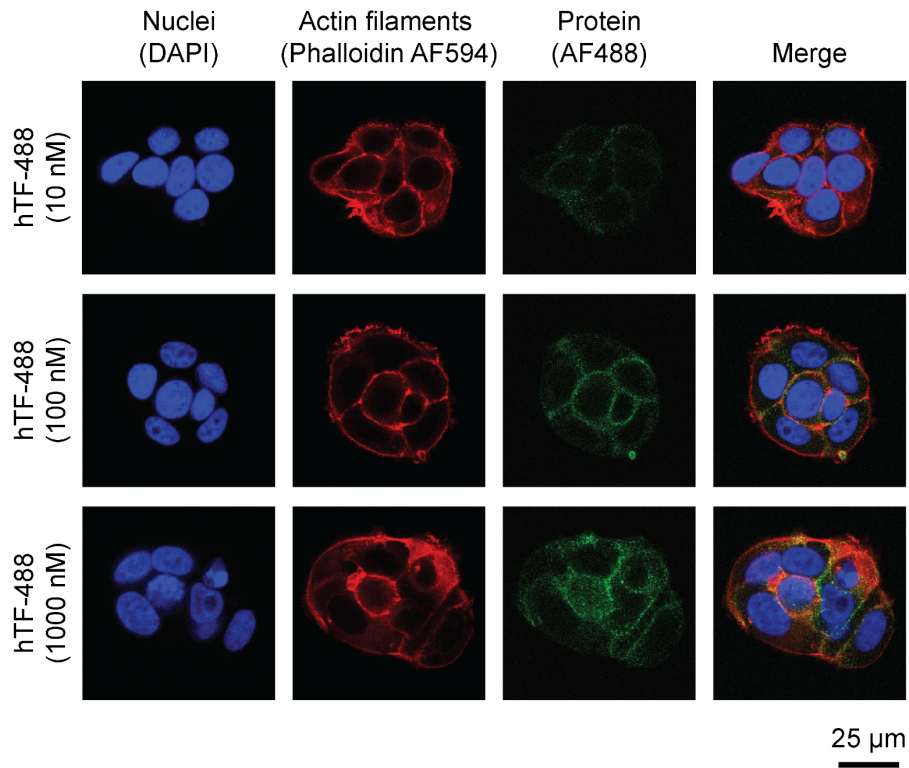
71 **Figure S2**



72
73

74 **Figure S2. MCF-7 cells express TFR and bind hTF.** (A) MCF-7 cells, which are a human breast
75 cancer cell line, express high levels of transferrin receptor (TFR) on their surface, as detected by
76 an anti-human TFR antibody directly conjugated to fluorescein and analyzed by flow cytometry.
77 (B) The binding of hTF to TFR was measured as the dissociation constant (K_D) using an
78 equilibrium binding assay. MCF-7 cells were incubated with a range of concentrations of hTF
79 directly labeled with Alexa Fluor 488 (hTF-488). The assay was performed in experimental
80 triplicate. Data from each replicate were fit to a sigmoidal curve, and the K_D value was calculated
81 for each replicate. The K_D is reported as the mean \pm standard deviation. A representative binding
82 curve is shown.

83 **Figure S3**
84



85 **Figure S3. hTF-488 internalization into MCF-7 cells is concentration dependent.** MCF-7
86 cells, which are a human breast cancer cell line, express high levels of transferrin receptor (TFR)
87 on their surface. Fluorescently labeled holo-transferrin (hTF-488) is internalized into the cells after
88 incubation for 1 h at 37 °C. Increasing the concentration of hTF-488 from 10 nM to 100 nM to
89 1000 nM (rows 1, 2, and 3) shows increasing internalization, as visualized by increasing green
90 signal within the cell boundaries. Blue indicates DAPI stain for cell nuclei; red indicates phalloidin
91 conjugated to Alexa Fluor 594, which stains actin filaments and helps to identify cell boundaries;
92 and green indicates the protein fluorophore conjugate labeled with Alexa Fluor 488. Scale bar
93 shown applies to all images.
94

95 **Description of supporting information videos.** To confirm the internalization of hTF-488 and
96 hTF-PVDMA_{rc}-mTEG, a series of consecutive focal planes were collected with confocal
97 microscopy, referred to as z-stack series, using a step size of 0.5 μ M. The data are available as .avi
98 video files in Supporting Information. In the videos, we observe that at the surfaces of the cells,
99 we predominantly see phalloidin staining of actin filaments, indicated in red. For both the hTF-
100 488 positive control molecule (SI_Video_1_hTF-488) and the hTF-PVDMA_{rc}-mTEG protein-
101 polymer conjugate (SI_Video_2_hTF-PVDMA-FC-mTEG), we see that the fluorophore, shown
102 in green, is contained within the cell boundaries, rather than at the cell surface, confirming
103 internalization of molecules. Blue indicates cell nuclei, stained with DAPI.